Impact of deoxygenation and warming on global marine species in the 21st century

Anne L. Morée[1,2], Tayler M. Clarke[3], William W. L. Cheung[3], Thomas L. Frölicher[1,2]

[1]Climate and Environmental Physics, Physics Institute, University of Bern, Bern, 3012, Switzerland
[2]Oeschger Centre for Climate Change Research, University of Bern, Bern, 3012, Switzerland
[3]Institute for the Oceans and Fisheries, The University of British Columbia, Vancouver, BC V6T 1Z4, Canada

Correspondence to: Anne L. Morée (anne.moree@unibe.ch)

Abstract. Ocean temperature and dissolved oxygen shape marine habitats in interplay with species' physiological characteristics. Therefore, the observed and projected warming and deoxygenation of the world's oceans in the 21st century may strongly affect species' habitats. Here, we implement an extended version of the Aerobic Growth Index (AGI), which quantifies whether a viable population of a species can be sustained in a particular location. We assess the impact of projected deoxygenation and warming on the contemporary habitat of 47 representative marine species covering the epipelagic, mesopelagic, and demersal realms. AGI is calculated for these species for the historical period and into the 21st century using bias-corrected environmental data from six comprehensive Earth System Models. While habitat viability decreases nearly everywhere with global warming, the impact of this decrease is strongly species-dependent. Most species lose less than 5% of their contemporary habitat volume over the 21st century at 2°C of global warming relative to preindustrial, although some individual species are projected to incur losses 2-3 times greater than that. We find that the in-habitat spatiotemporal variability of O_2 and temperature (and hence AGI) provides a quantifiable measure of a species' vulnerability to change. In the event of potential large habitat losses (over 5%), species vulnerability is the most important indicator. Vulnerability is more critical than changes in habitat viability, temperature or pO_2 levels. Loss of contemporary habitat is for most epipelagic species driven by the warming of ocean water and is therefore elevated with increased levels of global warming. In the mesopelagic and demersal realms habitat loss is also affected by pO_2 decrease for some species. Our analysis is constrained by the uncertainties involved in species-specific critical thresholds, which we quantify, by data limitations on 3D species distributions as well as by high uncertainty in model O_2 projections in equatorial regions. Focus on these topics in future research will strengthen our confidence in assessing climate-change driven losses of contemporary habitat across the global oceans.

1 Introduction

Ocean temperature and dissolved oxygen (O_2) are strongly linked by physical and biogeochemical processes as well as through their effects on the aerobic performance of aquatic ectotherms (Pörtner, 2010; Verberk et al., 2011; Breitburg et al., 2018; Oschlies et al., 2018; Seibel et al., 2021). Indeed, temperature and O_2 are both found to be central in shaping species' distributions and are important climatic stressors to marine species worldwide (Perry et al., 2005; Doney et al., 2011;

Poloczanska et al., 2013; Breitburg et al., 2018; Penn et al., 2018; Deutsch et al., 2020; Clarke et al., 2021). Observed and projected warming and deoxygenation are therefore likely to impact species.

Robust observational evidence of anthropogenically-forced deoxygenation is now becoming available as long-term O_2 changes emerge from their natural variability (Frölicher et al., 2009; Long et al., 2016; Stramma et al., 2020; Buchanan and Tagliabue, 2021; Sharp et al., 2022). Specifically, an increase in the temporal and spatial resolution of observational data has allowed for the discovery and quantification of a ~2% decline in the global top-1000m O_2 inventory since the 1960s (Ito et al., 2017; Oschlies et al., 2017; Schmidtko et al., 2017; Breitburg et al., 2018). This negative trend is projected to continue during the 21st century for all climate scenarios (Bopp et al., 2013; IPCC, 2019; Kwiatkowski et al., 2020). More than 10% of deep ocean O_2 is likely to be lost even if CO_2 emissions were stopped in the year 2020 (Oschlies, 2021). Earth System Model simulations project an O_2 loss between 100-600 meter depth of 13.27±5.28 mmol m^{-3} for a high-emission low-mitigation SSP5-8.5 scenario and 6.36±2.92 mmol m^{-3} loss for a low-emission high-mitigation SSP1-2.6 scenario by the end of the 21st century (2080-2099 mean values relative to 1870–1899 ± the inter-model standard deviation; Kwiatkowski et al., 2020).

However, simulated trends seem to underestimate trends in observations (Andrews et al., 2013; Oschlies et al., 2017; Oschlies et al., 2018; Buchanan and Tagliabue, 2021) and models poorly represent tropical Pacific Oxygen Minimum Zones (Cocco et al., 2013; Cabré et al., 2015), indicating the possibility of even stronger trends of deoxygenation toward the future.

Ocean temperatures are changing as well: Ocean warming is a direct effect of atmospheric warming, as the ocean takes up approximately 90% of the excess heat from anthropogenic activities (Von Schuckmann et al., 2020). Global mean sea surface temperatures are observed to have increased by ~0.5 °C since the 1960s (Hersbach et al., 2020). Earth System Model simulations project sea surface warming of 3.5±0.8°C for a high-emission low-mitigation SSP5-8.5 scenario and 1.42±0.32°C warming for a low-emission high-mitigation SSP1-2.6 scenario by the end of the 21st century (2080–2099 mean values relative to 1870–1899; Kwiatkowski et al., 2020). Most marine species will thus experience further warming of their habitat, considering that chances of limiting global atmospheric warming to 1.5°C are low even if all unconditional pledges by countries are implemented in full and on time (IPCC, 2021; Meinshausen et al., 2022). Models that include more complex representations of species biology and ecology show that every tenth of a degree of global warming increases impacts on marine biodiversity, transforming species assemblages through changes in abundance, biomass and catch potential (Cheung et al., 2016). Moreover, the warming signal penetrates the deep ocean where it has major potential to affect marine ecosystems together with deoxygenation and ocean acidification (Levin and Le Bris, 2015).

From a biogeochemical perspective, changes in O_2 content of a water parcel are driven by a combination of a) changes in O_2 solubility due to changes in temperature and salinity, b) changes in ventilation and stratification of the water column and associated changes in O_2 supply, c) changes in the partial pressure of O_2 (pO_2) due to gas diffusion rates that depend on temperature, and d) changes in large-scale biological consumption of O_2 (Keeling et al., 2010; Kwiatkowski et al., 2020; Buchanan and Tagliabue, 2021; Oschlies, 2021; Pitcher et al., 2021). The relative importance of these mechanisms for deoxygenation varies in space and time (e.g., Frölicher et al., 2009; Keeling et al., 2010; Frölicher et al., 2020), which makes it challenging to attribute local deoxygenation to a single driver (Pitcher et al., 2021). Generally, O_2 has reduced over the past

~60 years due to a combination of a-c in the extratropical oceans, while changes in large-scale biological consumption of O_2 (d) also contributed to changes in O_2 in low-O_2 equatorial zones (Buchanan and Tagliabue, 2021; Oschlies, 2021). Solubility effects dominate the top-200 meter deoxygenation while biological processes and especially ventilation changes increase their importance with depth (Schmidtko et al., 2017).

Consequences of the observed and projected deoxygenation and warming for marine species can be understood from the biogeochemical and physiological balance between pO_2 supply and demand, both of which depend on temperature (Pörtner and Knust, 2007; Verberk et al., 2011; Deutsch et al., 2015; Deutsch et al., 2020; Clarke et al., 2021). pO_2 supply to a water parcel and hence to a species is governed by a-d, while a species' O_2 demand (respiration) increases with temperature (Sect. 2.1).

This study uses the Aerobic Growth Index (AGI; Clarke et al., 2021) to quantify the combined effects of deoxygenation and warming on marine species in the 21st century. AGI is a species-specific ratio between pO_2 supply and demand and is interpreted as a measure of habitat viability. Viable habitat is characterized by a pO_2 supply over pO_2 demand ratio (i.e., AGI) sufficient for feeding, movement, defense, as well as growth and thus allows for sustainably maintaining a certain species' population (Clarke et al., 2021). Considering the ongoing deoxygenation and warming, AGI and hence habitat viability are expected to decrease (Deutsch et al., 2015; Clarke et al., 2021; Gruber et al., 2021; Oschlies, 2021). Our approach newly includes depth variability as well as temporal variability of temperature and O_2 in calculating AGI (Sect. 2.1), which we apply to 47 representative species thanks to the generalized temperature dependence of pO_2 demand in AGI (Sect. 2.2). For environmental data of temperature and pO_2 we use bias corrected Earth System Model projections from the latest version of the Coupled Model Intercomparison Project Phase 6 (CMIP6) (Sect. 2.3). Through this approach we assess the potential loss of viable contemporary habitat volume due to warming and deoxygenation for a representative selection of species - as well as identifying the drivers of such losses (Sect. 3).

2 Methods and data

2.1 Aerobic Growth Index

We apply the Aerobic Growth Index (AGI; Clarke et al., 2021) to quantify species-specific impacts on habitat viability in response to changes in temperature and pO_2. We interpret AGI as a measure of habitat viability. AGI integrates growth theory, metabolic theory, and biogeography to calculate a theoretical ratio of pO_2 supply over pO_2 demand for each species i (Eq. 1; rewritten from Eq. 14 in Clarke et al., 2021).

$$AGI_i = \frac{pO_2^{supply}}{pO_{2,i}^{demand}} = \frac{pO_2^{supply}}{pO_{2,i}^{threshold} \cdot \left(\frac{W_i}{W_{\infty,i}}\right)^{1-d} \cdot \exp\left(\frac{j_2 - j_1}{T_i^{pref}} - \frac{j_2 - j_1}{T}\right)} \quad (1)$$

Here, the environmental state is described by pO_2^{supply} (mbar) and T as in-situ temperature (K). The variables j_1 (the anabolism activation energy divided by the Boltzmann constant, 4500K), j_2 (the catabolism activation energy divided by the Boltzmann

constant, 8000K), and d (the metabolic scaling coefficient, 0.7) are species-independent to facilitate its application to a large number of species (Pauly, 2010; Cheung et al., 2011; Pauly and Cheung, 2018; Clarke et al., 2021). We note that the ratio between the mean species' weight W_i (g) and the species' asymptotic weight $W_{\infty,i}$ (g), $\frac{W_i}{W_{\infty,i}}$, reduces to $\frac{1}{3}$ as $W_i = \frac{1}{3} \cdot W_{\infty,i}$ (Clarke et al., 2021).

We newly consider both vertical and temporal variability in pO_2 and temperature in the calculation of the species' pO_2 threshold ($pO_2^{threshold}$; mbar) and preferred temperature (T^{pref}; K). Critical pO_2 values as well as preferred temperatures are highly species-dependent (Vaquer-Sunyer and Duarte, 2008; Pörtner and Peck, 2011; Seibel, 2011). Following Clarke et al. (2021) and Penn et al. (2018), we take $pO_2^{threshold}$ (T^{pref}) as the volume-weighted 10th (50th) percentile of all in-habitat pO_2 (temperature) values. AGI can therefore be calculated for any species for which we have distribution data as well as environmental data for temperature and pO_2. Temporal variations in pO_2 and temperature are considered by using monthly climatological mean data from the World Ocean Atlas 2018 (WOA18 average of all available decades; Boyer et al., 2018; Garcia et al., 2019; Locarnini et al., 2019; Zweng et al., 2019). The horizontal distribution data are extended over the full depth range of each species to include the vertical variability of O_2 and temperature in our estimate of $pO_2^{threshold}$, T^{pref} and hence AGI. The 0-200m depth range is used for epipelagic species, 200-1000m for mesopelagic species and the bottom layer of the ocean for the demersal species, thereby covering both deep and shallow demersal habitats (see Fig. C1 and Sect. 2.3). This approach facilitates the estimation of species-specific, temperature-dependent critical pO_2 levels and T^{pref} despite the lack of observational data from multi-stressor laboratory experiments that apply to field conditions (Boyd et al., 2018; Collins et al., 2022). Different iterations of the metabolic index (Deutsch et al., 2015; Penn et al., 2018; Deutsch et al., 2020), which require laboratory-based estimates of temperature-dependent critical pO_2 levels, agree well with AGI in their assessment of habitat loss (Clarke et al., 2021) despite the much fewer data needed to calculate AGI. For additional details on the calculation of AGI we refer to Clarke et al. (2021).

An AGI of one implies that there is sufficient O_2 supply for feeding, movement, and defence, but not growth and reproduction. To sustain a viable population, additional aerobic scope is needed until AGI is above its critical value (AGI^{crit}) for a particular species. Following Clarke et al. (2021), AGI^{crit} is the 10th percentile of all AGI values in a species' habitat including vertical and temporal variability as done similarly for $pO_2^{threshold}$ and T^{pref}. In this study a species is deemed impacted by changes in temperature and pO_2 whenever AGI drops below AGI^{crit} on an annual mean basis. All species information is listed in Table A1. The coarse resolution and the imperfect harmonization between the biogeographical, temperature and O_2 data may affect the accuracy of the estimated AGI^{crit}, as indicated by some species having AGI^{crit}, at or below 1. We discuss in Sect. 4 how such biases may affect the results and conclusion, and how future studies can build on our results to improve the accuracy of the analysis.

Relative changes in AGI (AGI^{rel}) between time=t_1 and time=t_0 can be estimated from Eq. 2:

$$AGI^{rel} = \frac{\Delta AGI}{AGI(t_0)} = \frac{pO_2(t_1)}{pO_2(t_0)} \cdot \exp\left((j_2 - j_1) \cdot \left(\frac{1}{T(t_1)} - \frac{1}{T(t_0)}\right)\right) - 1 \quad (2)$$

where ΔAGI is AGI(t_1)-AGI(t_0). Relative changes are thus entirely species-independent (in contrast to the metabolic index of Deutsch et al., 2015) and are interpreted as relative changes in habitat viability. Eqs. 1 and 2 show that j_2-j_1 (8000-4500=3500K) modulates the influence of the temperature effect on AGI. We maintain a reference period 1995-2014 throughout this study (i.e., AGI(t_0) is the mean AGI over the years 1995-2014). Individual contributions from pO_2 and temperature to AGI^{rel} are calculated by keeping temperature or pO_2 constant at its 1995-2014 mean state when calculating AGI^{rel}.

2.2 Species data

AGI can be calculated for nearly a 1000 commercially exploited marine species due to the generalized temperature dependence of the pO_2^{demand}. This broad applicability of AGI allows us to select 47 representative species (n=47), which are chosen such that depth level, climatic zone (tropical and temperate) and body size are represented. In addition, we selected some pelagic and deep-water wide-ranging species that inhabit both tropical and temperate regions, as well as the hypoxia-tolerant species *Dosidicus gigas*. Three depth groups are represented through our selection: Epipelagic species (n=23) in the 0-200 meter depth range, mesopelagic species (n=6) in the 200-1000 meter depth range and demersal species (n=18) at the sea floor (bottom wet layer of the models; Sect 2.3). The representativeness of our species selection is assessed in Sect. 3.4. Species' $pO_2^{threshold}$, T^{pref} and AGI^{crit} are listed in Table A1. The contemporary species distributions are based on a gridded product from Close et al. (2006) and are assumed to represent the 1995-2014 mean state (Fig. C1).

2.3 Earth system model data

Environmental data of O_2, potential temperature and salinity for the years 1850-2100 are taken from the Coupled Model Intercomparison Project Phase 6 (CMIP6) multi-model ensemble (Eyring et al., 2016). Scenarios 'historical', 'SSP5-8.5' and 'SSP1-2.6' as well as the pre-industrial control simulation 'piControl' were used from the six models for which these environmental data were available: CNRM-ESM2-1, MPI-ESM1-2-HR, UKESM1-0-LL, IPSL-CM6A-LR, GFDL-ESM4, and CanESM5 (Appendix Table A2). All model data were horizontally regridded to a 1° regular grid before further post-processing.

To account for mean errors and model drift, both a drift correction and bias correction were performed. First, the bottom layer ('seafloor') O_2 ocean data were linearly detrended for piControl drift over the piControl years corresponding to the scenario years (1850 to 2100) as these trends are more than 10% of the scenario signal for some models. Drift in bottom layer temperature and salinity as well as upper water column O_2, salinity and temperature were negligible as compared to the scenario signals and therefore not accounted for. Secondly, we performed a mean bias correction (e.g., Maraun, 2016) on all model data by subtracting the 'present-day' monthly mean climatological bias (the difference between WOA18 data vertically interpolated to the respective model levels and the respective model's 1995-2014 monthly climatology) from the entire simulated timeseries. We used the available WOA18 climatological mean product for the sea floor data because WOA18 climatologies are only available at monthly resolution until 1500m depth. The extracted original spatial resolution of the WOA18 data is 1° for O_2 and 0.25° for temperature and salinity but these were all regridded to 1° to match the regridded model data grid. Note

that to calculate the temperature biases, the model potential temperature was converted to in-situ temperature. Finally, pO_2 was calculated following Sect. E by Bittig et al. (2018), which is based on earlier work (Benson and Krause, 1984; Garcia and Gordon, 1992; Sarmiento and Gruber, 2006), and includes pressure correction (Taylor, 1978) and the correction for water vapor pressure (Weiss and Price, 1980) in the calculation of pO_2 (Appendix B).

All results are presented at global warming levels (i.e., global mean air temperature at 2 m; e.g., Hausfather et al., 2022). In order to do so we first bias-correct modeled surface air temperatures such that the 1995-2014 global mean air temperature increase since 1850-1900 is 0.87 °C as observed (HadCRUT.5.0.1.0; Morice et al., 2021) in order to be consistent with the bias-corrected ocean temperature and oxygen data. We then find the first year where the 15-year running mean of these bias-corrected global mean surface air temperature data is greater than or equal to the warming level of interest and calculate the 15-year running mean at that year over the data for the analyses. For warming levels above 1.5ºC, we only use the results for SSP5-8.5 as not all models reach warming of more than 1.5ºC in SSP1-2.6.

3 Results

3.1 Global changes in warming, deoxygenation and habitat viability

Ocean temperature is projected to increase (Fig. 1a) and pO_2 to decrease (Fig. 1b) with global warming of the atmosphere. These changes occur in all three depth layers considered here and for all CMIP6 models. Noticeably, the response of ocean warming and deoxygenation to global atmospheric warming is approximately linear (Fig. 1). From a linear fit to the multi-model mean CMIP6 changes in Fig. 1 we find that the epipelagic realm warms the most with 0.50±0.03 °C per degree of atmospheric warming (standard deviation given across the individual model fits). This signal is dampened toward depth to 0.18±0.02 °C per degree of global warming in the mesopelagic realm and 0.08±0.01 °C per degree of global warming in the demersal realm (Fig. 1a). In addition to the warming, we find that the epipelagic realm loses 0.40±0.55 mbar of pO_2, the mesopelagic loses 1.35±0.89 mbar of pO_2 and the demersal realm loses 1.17±0.97 mbar of pO_2 on average and per degree global warming of the atmosphere (Fig. 1b). The largest changes in pO_2 are projected at depth in contrast to ocean warming. The warming and deoxygenation reduce AGI relative to its contemporary state (i.e., a negative AGI^{rel}; Fig. 1c), which we interpret as a loss of habitat viability (Sect. 2.1) that is independent of species (Eq. 2). In the epipelagic, AGI decreases 2.17±0.69 % per degree of global warming (Fig. 1c), while AGI decreases 2.33±1.64 % per degree of global warming in the mesopelagic realm. The demersal decrease in AGI is 0.86±0.48 % per degree of global warming, making it the least pronounced of the three studied depth intervals. The approximately linear response of marine warming, deoxygenation, and loss of habitat viability to global atmospheric surface warming (Fig. 1) highlights and confirms that any additionally realized atmospheric warming will affect the marine environment (Cheung et al., 2016).

The projected changes are independent of greenhouse gas emission pathway and only depend on the amount of global warming to a first degree. Even though our results in Fig. 1 are presented at warming levels, we here highlight that the scenario

determines the maximum changes in temperature, pO_2 and AGI^{rel} (Fig. C2): Relative to the 1850-1900 mean, global multi-model mean warming by 2081-2100 in SSP1-2.6 is limited to 1.14±0.28 °C in the epipelagic, 0.62±0.07 °C in the mesopelagic and 0.22±0.02 °C in the demersal realm. For SSP5-8.5 the changes are approximately doubled to 2.70±0.76 °C, 1.00±0.15 °C and 0.40±0.06 °C of warming, respectively. Deoxygenation is also much reduced in the low-emission scenario as compared to the high-emission SSP5-8.5 scenario by 2081-2100, although model uncertainty is larger here: Global mean pO_2 is reduced by at most 0.88±1.42 mbar in the epipelagic, 3.23±2.96 mbar in the mesopelagic, and 5.42±3.80 mbar in the demersal realm for SSP1-2.6 while maximum global mean deoxygenation is projected to be stronger in SSP5-8.5 with 2.27±2.85 mbar, 7.13±4.22 mbar and 5.61±4.23 mbar pO_2 loss respectively. The relative loss of habitat viability is 6.39 % lower in SSP1-2.6 than in SSP5-8.5 by 2081-2100 in the epipelagic (-11.58±4.48 % under SSP5-8.5 vs. -5.18±2.08 % under SSP1-2.6), 4.62 % lower in the mesopelagic (-11.48±7.50 % under SSP5-8.5 vs. -6.86±5.60 % under SSP1-2.6), and 0.90 % lower in the demersal realm (-4.23±1.90 % under SSP5-8.5 vs. -3.33±1.69 % under SSP1-2.6).

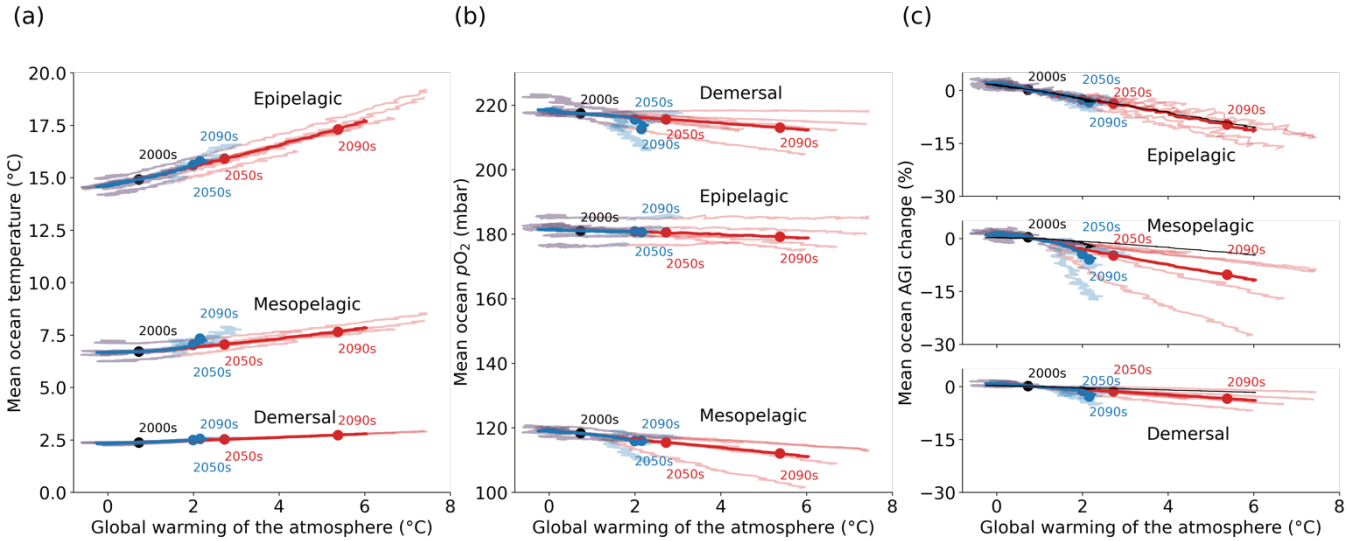

Figure 1 Simulated global mean changes in ocean in-situ temperature in °C (a), pO_2 in mbar (b) and AGI^{rel} in % (c) for different depth layers and global warming levels, where global warming is calculated as global surface air temperature increase relative to the 1850-1900 mean. The multi-model mean is given in opaque blue (SSP1-2.6) and red (SSP5-8.5) and has for several decades the corresponding 20-year multi-model mean year labelled. Individual models are shown in light blue and red without taking a running mean. AGI^{rel} is given relative to the 1995-2014 mean as in the remainder of the manuscript, and the mean contribution from temperature only (excluding the small effect of temperature on pO_2) is indicated by the black line in panel (c) and calculated by keeping pO_2 constant at its 1995-2014 mean state when calculating AGI^{rel}. AGI^{rel} is entirely species-independent (Eq. 2) and values that exceed 1000% or are below -1000% were excluded during the calculation of the global mean AGI changes to omit several grid-cells with extreme outliers caused by very small absolute changes in O_2 causing very large changes in AGI^{rel}.

3.2 Local changes and drivers of habitat viability

A relative reduction in habitat viability (i.e., a negative AGI^{rel}; Fig. 1c) is projected to occur almost everywhere at 2 °C of global warming (Fig. 2a-c; see Fig. C3 and C4 for 1.5 and 3 °C of global warming, respectively), indicating that for most

habitats and therefore species we expect a reduction in habitat viability. The relative reduction in habitat viability is generally larger in the epipelagic and mesopelagic realms (Figs. 1c, 2a, b), but the larger spatial heterogeneity at mesopelagic depths reveals that locally mesopelagic AGI reductions may far exceed those in the epipelagic, particularly in the North Pacific (Fig. 2b). Hence the location of a species' habitat, both vertically and horizontally, is key to projected changes in habitat viability for a specific species. Note that the patterns in each of the panels of Fig. 2 remain similar for higher degrees of global warming, only the intensity of change increases, which agrees with the approximately linear response of the global average AGI^{rel} to global warming (Fig. 1c).

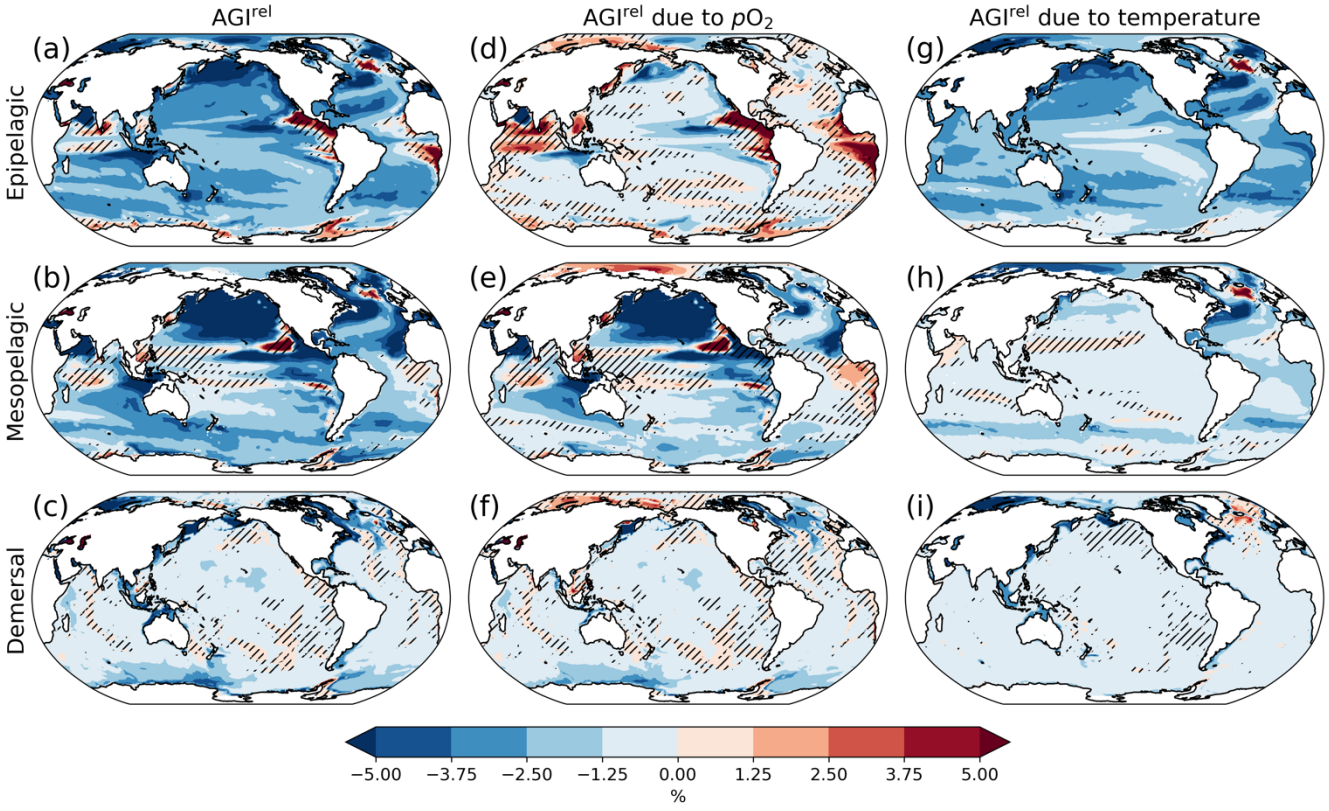

Figure 2 Multi-model mean AGI^{rel} relative to the 1995-2014 mean at 2 °C global warming (using SSP5-8.5 simulations), vertically averaged over the epipelagic and mesopelagic realms, and shown for the demersal realm (a-c). AGI^{rel} is divided into contributions from (d-f) pO_2 and (g-i) temperature. Data are hatched where more than 2 out of the 6 models disagree about the sign of change. Note that sea floor depth and thus demersal depth depend strongly on location. Contributions from pO_2 (temperature) are calculated by keeping temperature (pO_2) constant at its 1995-2014 mean state when calculating AGI^{rel}. Further note that since $[O_2]$ depends on temperature too, the contribution to AGI^{rel} from pO_2 also contains a minor temperature component.

When considering the contribution from the two drivers of AGI change, pO_2 and temperature changes, AGI^{rel} is driven mostly by temperature in the epipelagic and by pO_2 in the mesopelagic and demersal realms (Fig. 2d-i). The AGI^{rel} at 2 ºC of global warming due to pO_2 is -0.16±5.12% for the epipelagic, -2.52±6.96% for the mesopelagic, and -0.62±2.02% for the demersal realm (Fig. 2d-f), while the respective AGI^{rel} due to temperature are -2.32±1.36%, -0.91±1.18%, and -0.39±0.95% (Fig. 2g-i).

Hence, ~94% of AGI^{rel} is on average driven by the relatively pronounced warming in the epipelagic since changes in pO_2 are minor (Fig. 1b). This is because the epipelagic realm is generally well-ventilated with O_2-rich surface waters. For the mesopelagic (demersal), warming accounts for only 27% (39%) of the total AGI^{rel}. In the mesopelagic, the drivers of loss in habitat viability depend more strongly on location (Fig. 2e,h). The larger contribution from pO_2 to AGI^{rel} increases uncertainty for the mesopelagic and demersal realms because model projections are uncertain for pO_2 (Fig. 1b, C5). In some regions the effects of pO_2 and temperature on AGI^{rel} may compensate each other and result in negligible changes in AGI. We find examples of this in the Northern Indian Ocean at epipelagic depths, in the Gulf of Guinea at mesopelagic depths, and in the North Atlantic around Iceland at demersal depths.

AGI^{rel} has large model uncertainty for species having a large part of their habitat in eastern-boundary upwelling regions or around Antarctica at epipelagic depths, the western equatorial Pacific at mesopelagic depths, north of the equator in the Indian Ocean at epipelagic and mesopelagic depths or regions scattered across all ocean basins for demersal depths (hatched areas in Fig. 2a-c). Most of this uncertainty is coming from pO_2 (Fig. 2 d-f, Fig. C5), with temperature contributing to uncertainty in the North-Atlantic south of Greenland and in the western equatorial Pacific at mesopelagic depths. Exceptions to the decrease in AGI are limited to some small parts of the world's oceans including equatorial regions and the North-Atlantic south of Greenland in the epi- and mesopelagic, and around the Antarctic continent in the epipelagic. Model disagreement is generally large in these regions of positive AGI^{rel} and is mostly attributable to projected increases in pO_2 which have large uncertainties (hatching in Fig. 2a-f and model range in Fig. C5).

Besides considering the model uncertainty, we performed a sensitivity analysis of AGI^{rel} to the choice of generalized temperature dependence parameters (i.e., j_2-j_1). If j_2-j_1 is adjusted to represent an arbitrary low temperature sensitivity of 1000K, global mean AGI^{rel} is 34% of the standard case j_2-j_1=3500K in the epipelagic, 67% in the mesopelagic and 73% in the demersal realm. On the other hand, for an arbitrary high temperature sensitivity (j_2-j_1=6000K), global mean AGI^{rel} is 165% of the standard case j_2-j_1=3500K in the epipelagic, 118% in the mesopelagic and 126% in the demersal realm. Projections for epipelagic species are therefore most sensitive to the choice of j_2-j_1, as temperature changes are largest there. Further work is needed to explore the uncertainty in j_2 and j_1.

3.3 Impacts of AGI changes on habitat volume of individual species

The overall negative AGI^{rel} and hence relative loss of habitat viability with global warming (Figs. 1c and 2) causes loss of contemporary habitat volume (i.e., newly exposed volume with $AGI<AGI^{crit}$) for species at each of the studied depth ranges (Figs. 3 and 4). Habitat loss is expressed relative to its contemporary volume (Fig. 3) to facilitate comparison between wide-ranging and more narrowly distributed species. Loss of contemporary habitat is generally less than 15% at 2°C global warming, and mostly under 5%, but increases to up to ~25% for individual species at 3°C (Fig. 3). Wide-ranging epipelagic species (e.g., *Acanthocybium solandri*, *Coryphaena hippurus*, *Katsuwonus pelamis*, *Thunnus obesus*, or *Elagatis bipinnulata*; Fig. C1) experience losses of contemporary habitat volume of less than 5% for any of the analyzed warming levels, while more narrowly distributed species experience the largest losses of up to ~25% of their contemporary habitat at 3°C global warming (e.g.,

Micromesistius poutassou, *Thunnus atlanticus*, *Sebastes mentella*, or *Anarhichas denticulatus*). Notably, species that have the largest contemporary habitat loss at 1.5°C generally are those species that also lose the most at 3°C of global warming, which is in line with the earlier findings of approximately linear response of relative changes in habitat viability to warming and deoxygenation (Fig. 1). Any early (i.e., 1.5°C) response of a species to warming and deoxygenation is therefore a warning indicator for additional loss of contemporary habitat at increased levels of global warming.

We separately assess the impact of the uncertainty of AGI^{crit} on these results by calculating habitat loss with an AGI^{crit} of a) minimum AGI, b) 5^{th} percentile, c) 10^{th} percentile (i.e., the default case), d) 15^{th} percentile and e) 20^{th} percentile of in-habitat AGI. We find that even when including much higher thresholds (AGI^{crit} as 20^{th} percentile), our results are similar with a few species having large losses but most losing less than 5% at 2°C of warming relative to the 1995-2014 state (Fig. C6). Moreover, a sensitivity analysis for species *Thunnus atlanticus* and *Gadus morhua* shows that our median result is robust to the choice of the generalized temperature dependence parameters j_2-j_1 (we explored j_2-j_1 ± 71%; Fig. C7).

Absolute losses in habitat volume (i.e., loss expressed in volumetric terms instead of a percentage) show that small relative losses (Fig. 3) often correspond to the largest volumetric losses (Fig. 4). As an example, median *Thunnus alalunga* habitat loss is less than ~2.5% at any of the analyzed warming levels (Fig. 3), while absolute losses are the largest of all 47 species ranging from 0.25 to $1.5e^6$ km^3 depending on the global warming level (Fig. 4). On the other hand, we find species like *Sebastes mentella* for which relative losses are large (median 8-26% of the contemporary habitat depending on global warming level; Fig. 3) while absolute losses are comparably small (0.6-$1.8e^5$ km^3) because the contemporary volume of *Sebastes mentella* is relatively small (Fig. 4). Note that epipelagic species lose habitat volume in the order of a million km^3. In comparison, the entire Black Sea has a volume of about 0.5 million km^3. Depending on the location of viable contemporary habitat loss, for species of commercial interest such large absolute loss can be particularly impactful to local fisheries.

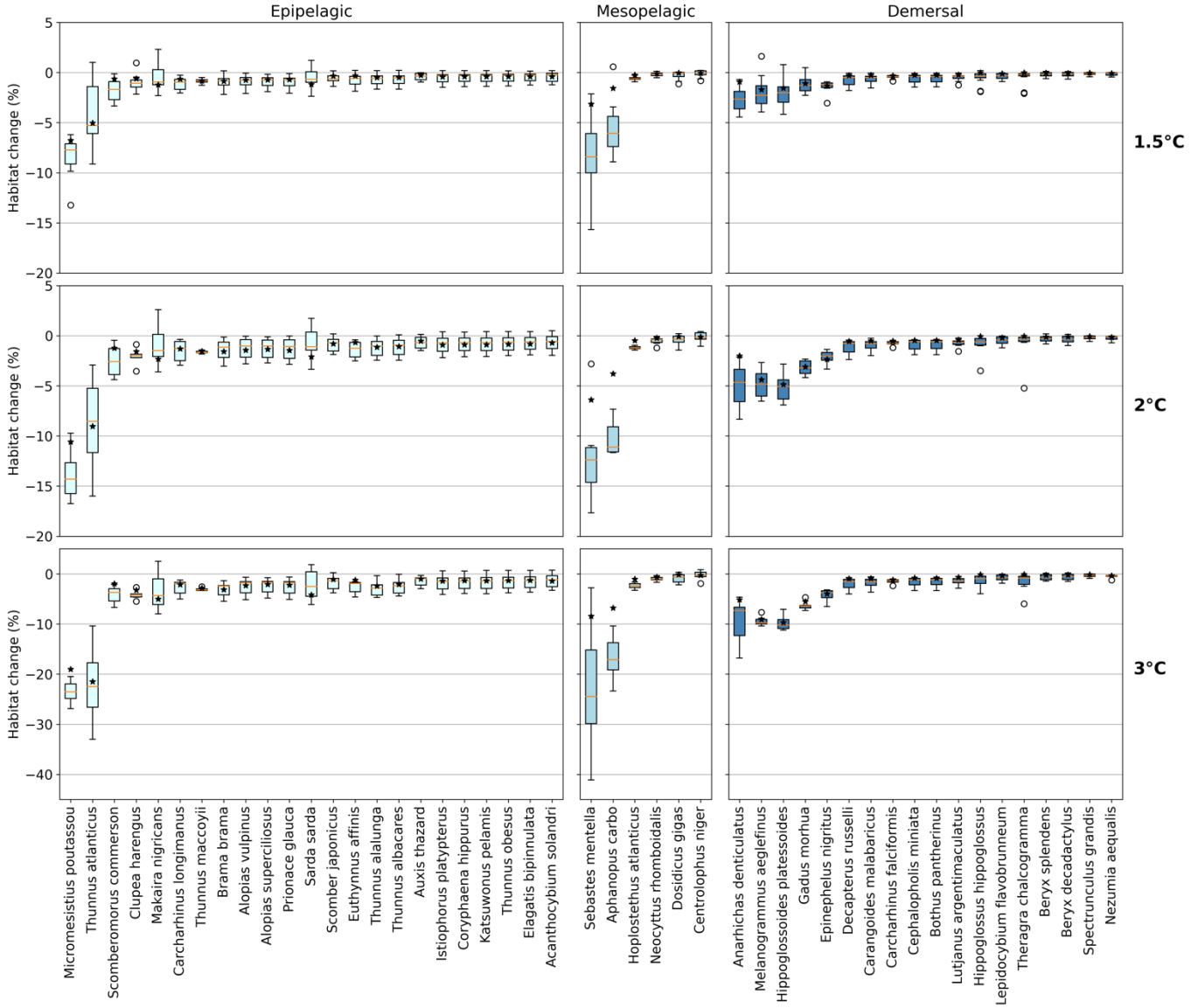

Figure 3 Habitat change (%) of contemporary (1995-2014) habitat volume for different levels of global warming, with negative values indicating habitat loss and positive values indicating habitat gain. Note the different y-axis scale for 3°C global warming. Habitat volume is considered lost when AGI<AGI^{crit} on an annual mean basis. For 1.5°C global warming both the SSP1-2.6 and SSP5-8.5 scenarios are included (number of datapoints n=2 scenarios * 6 models = 12 for each boxplot), while at higher levels of global warming we use SSP5-8.5 as not all models reach these warming levels under the SSP1-2.6 scenario (n=6 models). The species are ordered such that species with the largest median losses at 1.5°C global warming are on the left-hand side for each realm subplot. Each boxplot indicates the median in orange and a box bounded by the interquartile range (IQR; the 25th to 75th percentiles) and the whiskers extending to the data range with a maximum of 1.5×IQR, with outliers as open circles. Stars indicate the median contribution from temperature, the remainder is therefore due to pO_2 changes. As changes are expressed relative to the contemporary viable habitat volume (which is by definition 90% of the total habitat volume), values up to 10% (=100-90) are possible.

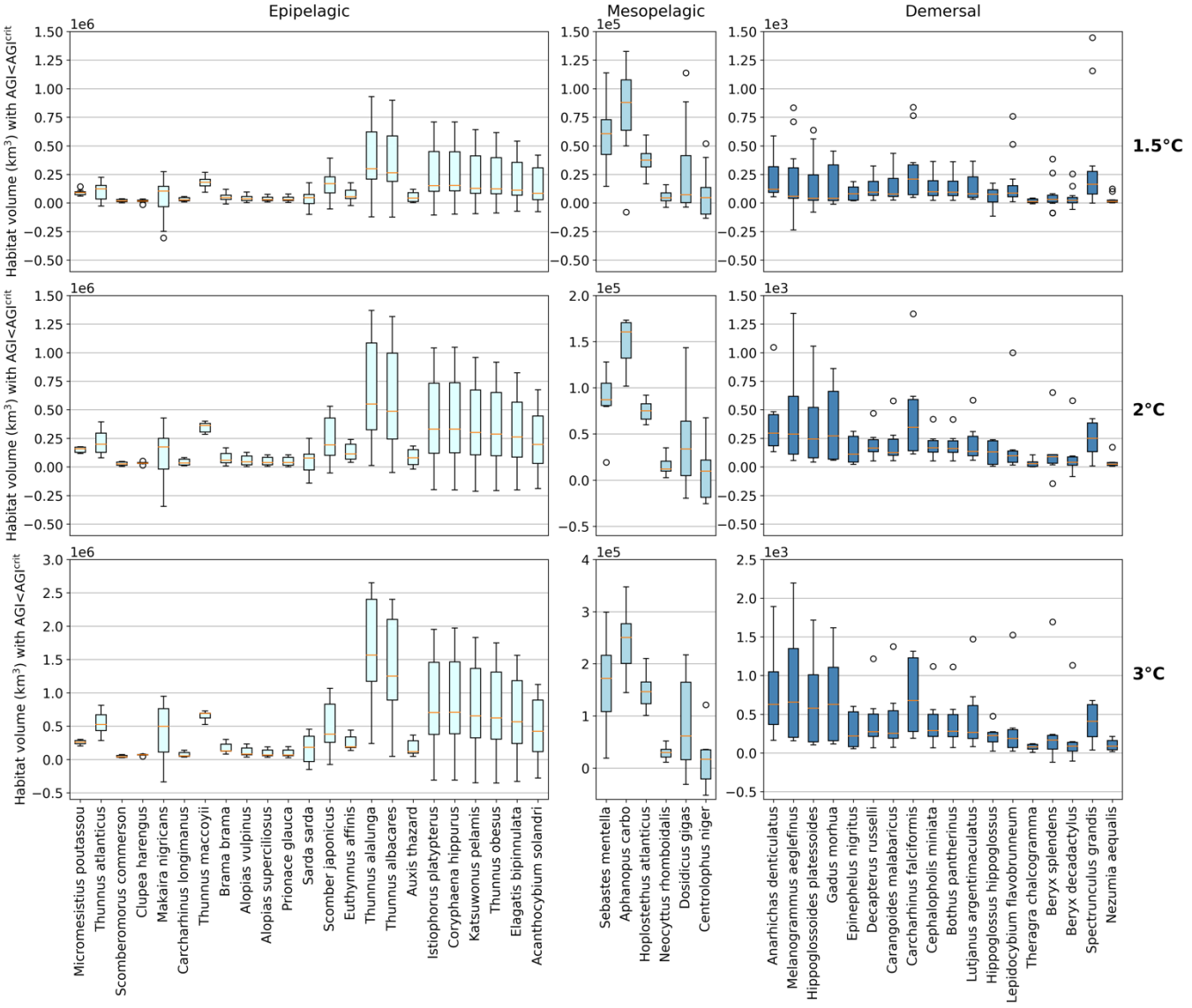

Figure 4 Contemporary habitat loss (km^3) for different levels of global warming. Note the different y-axes for both the depth groups and warming levels. Habitat volume is considerd lost when AGI< AGI^{crit} on an annual mean basis. For 1.5°C global warming both the SSP1-2.6 and SSP5-8.5 scenarios are included (number of datapoints n=2 scenarios * 6 models = 12 for each boxplot), while at higher levels of global warming we use SSP5-8.5 as not all models reach these warming levels under the SSP1-2.6 scenario (n=6 models). Species are ordered as in Fig. 3. Each boxplot indicates the median in orange and a box bounded by the interquartile range (IQR; the 25th to 75th percentiles) and the whiskers extending to the data range with a maximum of 1.5×IQR, with outliers as open circles.

For most species, temperature is the main driver of habitat loss (black stars in Fig. 3). Exceptions exist for example in the mesopelagic, where pO_2 drives about half of the habitat loss for the two species with the largest loss (i.e., *Sebastes mentella* and *Aphanopus carbo*) as well as for the demersal species *Anarhichas denticulatus*. Even though most of the loss can be explained by warming, not all species have large losses despite warming being relatively uniform although dampened toward

depth (Kwiatkowski et al., 2020). These differences can be explained by considering the original spatial and temporal pO_2 and temperature variability in each species' habitat, which shapes their vulnerability to change. This is investigated next.

3.4 Drivers of habitat volume loss of individual species

The differences in habitat loss between species as shown in Figs. 3 or 4 are better understood from the probability density of contemporary (1995-2014) in-habitat AGI for each species (conceptual Fig. 5 and species results in Fig. C8). The spatial variability of the contemporary pO_2 and temperature in each species' habitat results in a species-specific probability density function (PDF) for AGI (black lines in Fig. 5a,b). Depending on this shape, a given reduction in AGI (ΔAGI) exposes a relatively large or small part of the species' habitat to subcritical AGI values (red lines and stippling in Fig. 5a,b), thereby causing volume loss.

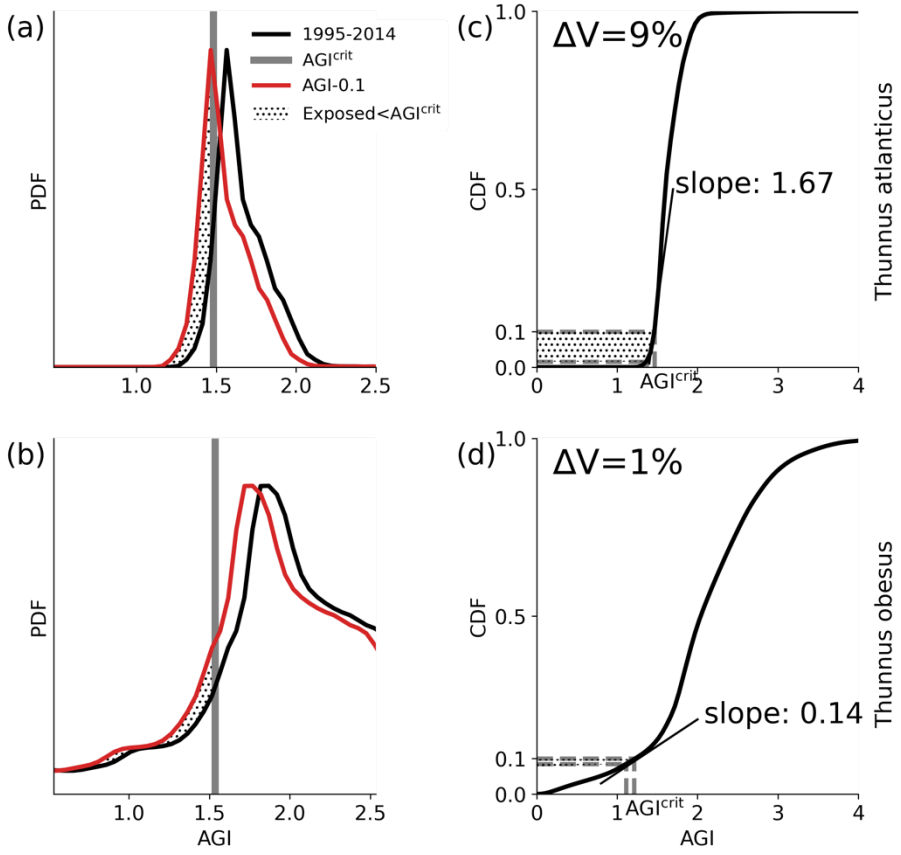

Figure 5 Conceptual figure based on *Thunnus atlanticus* (a,c) and *Thunnus obesus (b,d)* showing the difference in impact (change in volume ΔV) of an example mean AGI reduction of 0.1 (i.e., habitat-mean ΔAGI=0.1) below the 1995-2014 contemporary mean (black lines). This difference is shown to be related to the shape of the PDF and the slope of the CDF at 0.1 (i.e., at AGI^{crit}), which we refer to as the species' "vulnerability".

We can quantify the "vulnerability" of a species to changes in AGI by calculating the cumulative sum of the PDFs (i.e., the cumulative density function CDF; conceptual Figs. 5c,d and species-specific results in C9). The slope of the CDF at a

cumulative density of 0.1 (i.e., 10% of the volume where AGI^{crit} is defined) indicates the potential loss in habitat for a certain change in AGI (Fig. 5 and C9). If the slope of the CDF is steep at the critical threshold, the species is relatively vulnerable to warming and deoxygenation as only a small reduction in habitat viability (i.e., AGI) will push a relatively large volume below the critical threshold. An example is given in Fig. 5, where for an identical change in mean in-habitat AGI of 0.1 just 1% of the volume is pushed below AGI^{crit} for a species with a small slope of 0.14 (Fig. 5b,d, '*Thunnus obesus*'), while the same change in AGI results in 9% volume loss for a species with a large slope of 1.67 (Fig. 5a,c, '*Thunnus atlanticus*'). Changes in the slope of some species' CDFs indicate that different vulnerabilities exist for different parts of that species' habitat (Fig. C9). Hence, in habitat areas that are represented by a part of the CDF with a relatively steep slope, a relatively small change in AGI is needed to bring a relatively large volume closer to AGI^{crit}. Only the CDF slope at AGI^{crit} relates directly to viable habitat volume loss as only AGI values below AGI^{crit} are considered to have an impact on habitat volume.

Indeed, projected habitat volume loss increases with species' vulnerability (i.e., the CDF slope at AGI^{crit}; Fig. 6d), as well as to a lesser extent with warming and deoxygenation (Fig. 6b,c). Notably, the largest absolute reductions of mean in-habitat AGI do not indicate those species who lose most contemporary habitat volume (Fig. 6a). On the contrary, the environmental state of the contemporary habitat as captured in the PDFs and thus the slope of the CDFs and vulnerability is the strongest indicator for impact: 87% of the variance in volume loss at 2 °C global warming can be explained by vulnerability (R^2 of linear fit in Fig. 6d). This result holds across different levels of global warming. At 1.5°C of global warming, 85% of the variance in volume loss can be explained by vulnerability, and at 3°C of global warming this is 88% (see Figs. C10 and C11).

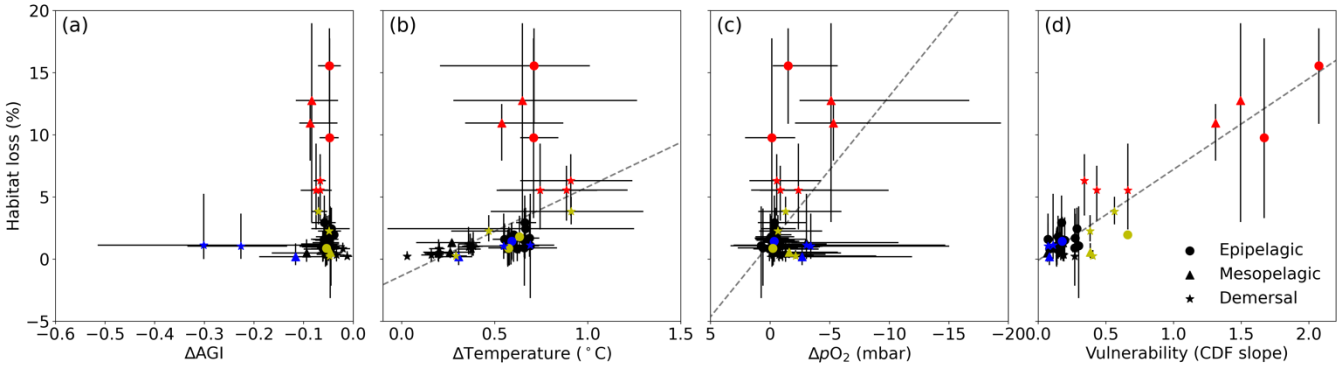

Figure 6 Multi-model mean in-habitat changes at 2°C of global warming of (a) AGI, (b) temperature, (c) pO_2 (in SSP5-8.5) and (d) vulnerability (CDF slope at a cumulative density of 0.1 based on 1995-2014 mean data, Fig. C9) plotted against loss of contemporary habitat volume for each species (model range indicated by error bars). Species with > 5% loss marked in red, more than –0.1 ΔAGI in blue, and volume loss < 5% as well as vulnerability > 0.3 in yellow. There is no uncertainty in the vulnerability calculation because all models have the same 1995-2014 CDF slope due to the WOA18 bias-correction. From a linear regression to the data which is plotted in dashed grey we find an R^2 of 0.0% for (a) which line is therefore not plotted, 18% for (b), 21% for (c) and 87% for (d).

Habitat viability strongly depends on the variability of temperature and O_2 in the habitat of the species as captured by the species' vulnerability (Figs. C9 and 6d). Therefore, reports of relative losses in habitat viability based on pO_2 supply over pO_2 demand ratios (e.g., Deutsch et al., 2015; Oschlies, 2021) should not be interpreted as leading to actual reductions of viable habitat for individual species as they do not include species-specific thresholds nor their vulnerabilities.

We highlight three groups of species for further discussion of the results at 2°C of global warming: (1) The most affected and vulnerable species due to high vulnerability despite small ΔAGI (red markers in Fig. 6): *Micromesistius poutassou*, *Thunnus atlanticus*, *Sebastes mentella*, *Aphanopus carbo*, *Anarhichas denticulatus*, *Melanogrammus aeglefinus* and *Hippoglossoides platessoides*, (2) the resilient species which have low losses despite high ΔAGI due to low vulnerability (blue markers in Fig. 6): *Centrolophus niger*, *Hippoglossus hippoglossus* and *Theragra chalcogramma*, and (3) the vulnerable, but not affected species who lose <5% of their habitat volume due to small ΔAGI despite relatively high vulnerability (yellow markers in Fig. 6): *Clupea harengus*, *Thunnus maccoyii*, *Neocyttus rhomboidalis*, *Epinephelus nigritus*, *Gadus morhua* and *Nezumia aequalis*. Considering the range captured in Fig. 6a-d we expect that our selection of species is representative of a wide range of marine ectotherms.

Interestingly, species with high vulnerability and loss (red markers in Fig. 6) all have a high $pO_2^{threshold}$ above ~150 mbar (Table A1, Fig. C12). Thus, even though warming explains most of the loss of contemporary habitat, loss is only high for vulnerable species (Fig. 6d) – which in turn all are sensitive to pO_2 as evidenced by their $pO_2^{threshold}$ above ~150 mbar (Fig. C12). A high sensitivity to pO_2 and hence a high $pO_2^{threshold}$ is therefore an indicator of vulnerability, although not all species with high $pO_2^{threshold}$ are vulnerable (Fig. C12). The high vulnerability for species with a high $pO_2^{threshold}$ shows that also species in well-oxygenated regions can be vulnerable to climate change as their natural pO_2 range is limited. We further note that vulnerability does not depend on the depth realm of a species. Resilient species (blue markers in Fig. 6) have strong spatiotemporal variability of AGI (broad PDF in Fig. C8) such that even large mean changes of AGI (Fig. 6a) do not expose a large volume to subcritical AGI values. Noticeable is that the two species with a PDF skewed to the right (Fig. C8; *Hippoglossus hippoglossus* and *Theragra chalcogramma*) are both in this group, while all other species tend to have a left-skewed PDF of AGI values in their habitat. These two species are both demersal-dwelling and are very pO_2 tolerant (i.e., low $pO_2^{threshold}$; Table A1) and have a wide range of different AGI values in their habitat, with a relatively large volume of high-AGI values causing the right skew (Fig. C8) and resilience (Fig. C12). Whether AGI is the right metric for determining habitat viability for these two species needs further investigation that goes beyond the scope of this study. The six species with relatively high vulnerability but small habitat losses (yellow markers in Fig. 6) experience relatively small AGI changes in their habitats even at 3°C global warming (Fig. C8) thereby preventing large habitat losses.

4 Discussion

We introduce a new version of AGI that adds vertical temporal variability in the calculation of $pO_2^{threshold}$, T^{pref}, and AGI^{crit}, which makes it possible to assess volumetric habitat changes. The original AGI applies and assesses temporal variability in the horizontal direction only (surface or bottom ocean layers for pelagic and demersal species, respectively; Clarke et al., 2021), as commonly practiced (e.g., Bryndum-Buchholz et al., 2019; Tittensor et al., 2021). In other words, either surface or sea floor data were applied for the calculation of $pO_2^{threshold}$, T^{pref}, AGI^{crit} and hence AGI in earlier work. To assess the differences between our new approach and the original approach we repeated the analysis as presented in Fig. 3, now using

surface ocean data only for mesopelagic and epipelagic species as well as calculating $pO_2^{threshold}$, T^{pref}, AGI^{crit} from the surface monthly mean WOA18 data only (Fig. C13). We find that the sensitivity to global warming of all species is higher for the original AGI as compared to our new approach which includes vertical and seasonal variability of temperature and pO_2. This is understood from the combination of a) limited spatial variability of surface ocean pO_2 as well as temperature, leading to higher T^{pref} and $pO_2^{threshold}$ estimates and therefore stronger sensitivity to warming and deoxygenation as compared to our new approach and b) larger AGI^{rel} changes closer to the surface. We expect that including temporal and vertical spatial variability in calculating AGI provides a more realistic estimate of the pO_2 and temperature variability experienced by a species and therefore a better estimate of its sensitivity to warming and deoxygenation. Nevertheless, we acknowledge that further increasing spatiotemporal resolution (e.g., using daily-mean data and including interannual variability) may increase variability (Deser et al., 2009; Baumann et al., 2015) which can affect estimates of T^{pref}, $pO_2^{threshold}$ and AGI^{crit}. Unfortunately, no established theory exists yet to decide what temporal variability in environmental parameters best captures species' T^{pref}, $pO_2^{threshold}$ or AGI^{crit}. By considering WOA18 monthly mean climatological data as the basis for our estimates of T^{pref}, $pO_2^{threshold}$ and AGI^{crit}, we are consistent with the time resolution of the CMIP6 model data (monthly mean).

Regarding the choice of the 10^{th} percentile threshold and impact of its uncertainty on our results (Fig. C6), we consider an AGI^{crit} threshold above the 20^{th} percentile of in-habitat AGI values unlikely as then by definition already 20 percent of the habitat would be unsuitable to sustain a viable population of that species. Nevertheless, for species where AGI^{crit} is very close to 1 or even below 1 (Table A1), a higher percentile may be warranted as a meaningful critical value. At the 10^{th} percentile, some uncertainty in the species-specific physiological parameters is considered. We find for most species that the 10^{th} percentile is located at an AGI above which habitat volume steeply increases suggesting it acts as an appropriate threshold (Fig. C8).

Regarding species' data, we assume that our results can be generalized to commercial fish and invertebrates worldwide, as they are based on representative species from different climatic zones (tropical, temperate, polar), vertical habitat (epipelagic, mesopelagic, demersal), geographic range breadths, taxonomic groups (fish and invertebrates) and size classes. Species distribution ranges were generated by an algorithm developed by the Sea Around Us project (see Close et al., 2006; Cheung et al., 2008). The resulting distributions, and the parameters used for their construction are available at http://www.seaaroundus.org. These distributions have been used to project climate-impacts on fishery resources in a great number of studies (Cheung et al., 2009; Cheung et al., 2010; Fernandes et al., 2013), and are assumed to represent species distributions over the period 1995-2014 (Tai et al., 2021). Our assumption to extend the 2D distributions provided by Close et al. (2006) over the entire depth range of each species' depth realm is driven by data sparsity and reliability of 3D species distributions for our selection of species. When reliable 3D habitats, or even time-varying habitats, can be constructed from species' observations these could be included (e.g., distribution data are continuously collected in the Ocean Biodiversity Information System but are currently too sparse to provide 3D distribution data). Some species may be limited to only part of their assigned depth range or live partly (and possibly temporarily) above or below it. Nevertheless, we expect that the assigned depth range

generally provides a good estimate of in-habitat pO_2 and temperature variability, which affects $pO_2^{threshold}$, T^{pref} and therefore AGI and AGI^{crit}.

Our results for the mesopelagic include two vertical migrators (*Dosidicus gigas* and *Aphanopus carbo*). As opposed to most other species, the distribution range of vertical migrators is limited at the cold boundary of the distribution because of their low aerobic scope in cold waters (Seibel and Birk, 2022). Therefore, the temperature sensitivity of these species is likely not captured by the generalized temperature dependence in AGI, and contemporary habitat loss due to warming and deoxygenation as estimated for *Aphanopus carbo* is likely overestimated. We nevertheless project negligible loss of contemporary habitat for *Dosidicus gigas* (Fig. 3) due to its low vulnerability and low $pO_2^{threshold}$, which is in good agreement with the findings of Seibel and Birk (2022) despite the generalized temperature dependence of AGI. Species-specific thresholds $pO_2^{threshold}$ and AGI^{crit} and preference T^{pref} are calculated based on the in-habitat spatiotemporal variability of pO_2, temperature and AGI respectively. This is done in lack of observation-based thresholds and preferences that translate to field conditions (Boyd et al., 2018; Collins et al., 2022). Detrimental effects from deoxygenation such as reduced vision actually become relevant at much higher pO_2 than (near) lethal pO_2 levels (Mccormick and Levin, 2017), while only the latter is often what is assessed in the lab. As an effect, the exact threshold of impact remains unknown and probably depends on many factors including the impact itself, and the abruptness, magnitude, intensity, duration, heterogeneity, and recurrence of exposure to subcritical values (Gruber et al., 2021), as well as timing of and adaptability to unfavorable temperatures, subcritical pO_2 and hence subcritical AGI.

Through the bias correction of the CMIP6 model data all monthly mean biases relative to WOA18 are removed from our analysis. We acknowledge the influence of observational uncertainties as well as resolution mismatch between our model and the observational WOA18 data used in our bias correction (Casanueva et al., 2020). More complex bias adjustment such as correction for variance biases is prevented by the spatial and temporal resolution of the model and observation data at the global scale. The ongoing effort to collect, compile, and quality-control O_2 data in open-access repositories (e.g., Grégoire et al., 2021) will hopefully make it possible to do more advanced bias correction in the future. Until that time the strong temporal variability and spatial heterogeneity of O_2 trends complicate the comparison between model and observational data. Nevertheless, the remaining forced response of the models likely underestimates deoxygenation (Andrews et al., 2013; Oschlies et al., 2017; Oschlies et al., 2018; Buchanan and Tagliabue, 2021) and overestimates atmospheric warming (Tokarska et al., 2020) and therefore ocean warming for some CMIP6 models. Part of these warming biases are due to the relatively high climate sensitivities in the CMIP6 models (Meehl et al., 2020). As a further measure to limit model uncertainty, we therefore present results at different global warming levels such that they are insensitive to the differences in model climate sensitivity (Hausfather et al., 2022). We last acknowledge the relatively coarse resolution of the CMIP6 data (typically ca. 100km in the ocean) which for species with a highly local distribution (Fig. C1) may lead to higher model uncertainties, especially along the coasts where model disagreement is larger (Fig. C5).

Our approach may give a conservative estimate of contemporary habitat loss since a) crossings of the critical thresholds on timescales shorter than a year are excluded from our analysis, b) CMIP6 projections likely underestimate deoxygenation (Andrews et al., 2013; Oschlies et al., 2017; Oschlies et al., 2018; Buchanan and Tagliabue, 2021), but considering the

importance of temperature in driving habitat loss (Fig. 3), especially in the epipelagic realm, the uncertainty of pO_2 projections likely has a relatively small effect on our results, and c) we do not include other potential stressors on species' habitats in our analysis such as acidification, changes in ecosystem structure, overfishing, marine phenology, disease pressure, food resources, predation pressure, pollution or eutrophication (e.g.; Poloczanska et al., 2016; Bindoff et al., 2019; Whalen et al., 2020). Examples of crossings of the critical thresholds on timescales shorter than a year would be short hypoxic events and marine heatwaves (Frölicher and Laufkötter, 2018; Jacox et al., 2020; Cheung et al., 2021). Projected deoxygenation and particularly hypoxic or anoxic events have the potential to worsen and even surpass the effects of warming, marine heatwaves, and acidification (Gruber et al., 2021; Sampaio et al., 2021). On the other hand, for some species the impact will be overestimated if they are able to adapt to future warming and deoxygenation (Cheung et al., 2009; Pinsky et al., 2013; García-Molinos et al., 2016; Palumbi et al., 2019; Collins et al., 2021; Liao et al., 2021). Further note that we considered potential loss of contemporary habitat only: Mobile species have been observed to redistribute based on the rate and direction of climate change (Pinsky et al., 2013) which can preserve the species range area if they are able to expand into newly suitable areas - however this can alter the original ecosystem structure and function.

For most species we find a loss of habitat volume of less than 10%. It is found for example by Gotelli et al. (2021) that only a small percentage of species drives the observed changes in marine species assemblages, showing that even when only a few species experience large losses, impacts can be profound for the ecosystem. For the individual species however, the loss of only a small fraction of their contemporary habitat likely provides adaptation opportunities. Our results imply that species that are deemed vulnerable due to their limited range of in-habitat pO_2 and temperature are likely to be the most impacted by global warming (i.e., 'vulnerable species' in Fig. 6 and species with steep CDF slopes in Fig. C9). Our study can therefore inform e.g., fisheries management by identifying species particularly vulnerable to ocean warming and deoxygenation. Such identification provides species-specific information complementing earlier studies that found reduced impact on fisheries at lower levels of global warming (Cheung et al., 2016). Indeed, for any additional global warming, our study shows increased marine deoxygenation and warming as well as increased loss of contemporary habitat across all species albeit with a strongly species-specific magnitude. These results confirm the need to limit global warming levels to the minimum to prevent loss of contemporary habitat and support the identification of the species that would be most vulnerable to marine deoxygenation and warming.

5 Conclusions

- Marine warming and deoxygenation are projected to intensify with global warming and drive a relative decrease in global habitat viability penetrating to all depths (Fig. 1 and 2).
- The generally negative relative changes in habitat viability (i.e., AGI^{rel}) are dominated by warming at the surface while deoxygenation becomes increasingly important with depth (Fig. 2).

- Species' loss of contemporary habitat is driven mostly by warming in the epipelagic realm, while in the mesopelagic and demersal realms reduced pO_2 is also contributing for some species (Fig. 3).
- Deoxygenation and warming cause most species to lose less than 5% of their contemporary habitat volume over the 21st century relative to preindustrial (Fig. 3). Some individual species are however projected to incur losses 2-3 times greater than that at 1.5 and 2 ºC of global warming and 4-5 times greater at 3ºC of global warming. At 2 ºC of global warming, epipelagic losses are generally in the order of 0.1-0.5 million km^3, while mesopelagic losses are 0.01-0.15 million km^3 and demersal losses are in the order of about 0.00025 million km^3.
- The impact of negative relative changes in habitat viability (i.e., AGI^{rel}: Figs. 1c and 2) on lost habitat volume (Figs. 3 and 4) depends on species' vulnerability (Figs. 5, 6d, C9).
- Species' vulnerability is shown to be the most important indicator for potential large (>5%) habitat losses - not relative or absolute changes in AGI, pO_2 or temperature (Fig. 6). A species' $pO_2^{threshold}$ above ~150 mbar is an indicator for high species vulnerability to warming (Fig. C12). Our approach of quantifying vulnerability can help identify those species most vulnerable to marine warming and deoxygenation.
- We introduce an updated version of AGI. By including temporal and vertical spatial variability in the calculation of the species-specific O_2 thresholds and temperature preference, we include a more realistic representation of the in-habitat variability of O_2 and temperature and therefore likely the species' tolerance to these. The updated AGI has lower sensitivity than in the original AGI of Clarke et al. (2021) (Figs. 3 and C13).

Appendix A Tables

Table A1 Species information, ordered alphabetically by species name. Group 1 is epipelagic; group 2 is mesopelagic, and group 3 is demersal. $pO_2^{threshold}$ (mbar), Tpref (°C) and AGI^{crit} (-) are based on the WOA18 monthly climatology in the habitat (Fig. C1) of the species except for species in the demersal group for which only a mean climatology is available (see also Sect. 2.2). The slope (change in fraction of total habitat volume per unit change in habitat-mean AGI at AGI^{crit}) is calculated from the species' CDF (Sect. 3.4).

Species	Group	$pO_2^{threshold}$	T^{pref}	AGI^{crit}	slope
Acanthocybium solandri	1	108.70	23.87	1.73	0.14
Alopias superciliosus	1	130.58	24.00	1.54	0.16
Alopias vulpinus	1	139.30	22.11	1.39	0.20
Anarhichas denticulatus	3	157.21	2.11	1.31	0.66
Aphanopus carbo	2	167.60	9.05	1.23	1.31
Auxis thazard	1	102.87	22.91	1.66	0.08

Beryx decadactylus	3	61.96	4.54	1.22	0.18
Beryx splendens	3	64.53	4.01	1.21	0.19
Bothus pantherinus	3	59.14	13.69	1.56	0.16
Brama brama	1	148.56	19.67	1.22	0.27
Carangoides malabaricus	3	63.66	16.39	1.73	0.16
Carcharhinus falciformis	3	89.78	2.90	1.03	0.27
Carcharhinus longimanus	1	126.28	25.17	1.62	0.15
Centrolophus niger	2	61.08	9.45	1.47	0.08
Cephalopholis miniata	3	58.51	14.05	1.60	0.15
Clupea harengus	1	197.80	6.23	1.10	0.29
Coryphaena hippurus	1	126.95	21.68	1.50	0.14
Decapterus russelli	3	60.18	14.10	1.56	0.17
Dosidicus gigas	2	36.09	9.68	1.43	0.07
Elagatis bipinnulata	1	120.27	23.10	1.62	0.14
Epinephelus nigritus	3	108.37	10.45	1.32	0.38
Euthynnus affinis	1	111.61	25.59	1.73	0.07
Gadus morhua	3	180.36	3.77	1.17	0.56
Hippoglossoides platessoides	3	166.72	5.06	1.29	0.34
Hippoglossus hippoglossus	3	45.47	2.43	1.39	0.07
Hoplostethus atlanticus	2	114.96	8.73	1.47	0.18
Istiophorus platypterus	1	127.49	21.88	1.50	0.14
Katsuwonus pelamis	1	124.89	22.27	1.55	0.14
Lepidocybium flavobrunneum	3	55.14	4.69	1.19	0.15
Lutjanus argentimaculatus	3	65.19	14.84	1.61	0.17
Makaira nigricans	1	135.23	20.88	1.53	0.30
Melanogrammus aeglefinus	3	174.00	5.09	1.21	0.43
Micromesistius poutassou	1	202.61	7.90	0.94	2.07
Neocyttus rhomboidalis	2	111.72	8.82	1.49	0.39
Nezumia aequalis	3	121.60	4.27	1.04	0.40
Prionace glauca	1	134.23	23.07	1.46	0.18
Sarda sarda	1	131.21	16.89	1.33	0.27
Scomber japonicus	1	121.70	20.11	1.48	0.13
Scomberomorus commerson	1	134.73	26.23	1.55	0.17
Sebastes mentella	2	174.62	2.74	1.34	1.50

Spectrunculus grandis	3	118.23	1.75	1.34	0.27
Theragra chalcogramma	3	35.08	2.08	1.31	0.11
Thunnus alalunga	1	141.59	19.75	1.33	0.18
Thunnus albacares	1	139.70	20.20	1.35	0.17
Thunnus atlanticus	1	174.86	25.65	1.48	1.67
Thunnus maccoyii	1	194.28	13.76	1.00	0.66
Thunnus obesus	1	124.90	22.15	1.53	0.14

Table A2 CMIP6 multi-model data used in this study.

Model name	Institute	References
CNRM-ESM2-1	CNRM: Centre National de Recherches Meteorologiques, Toulouse 31057, France CERFACS: Centre Européen de Recherche et de Formation Avancée en Calcul Scientifique, Toulouse 31057, France	SSP1-2.6 (Voldoire, 2019a) SSP5-8.5 (Voldoire, 2019b) historical (Séférian, 2018a) piControl (Séférian, 2018b)
MPI-ESM1-2-HR	MPI-M (historical and piControl): Max Planck Institute for Meteorology, Hamburg 20146, Germany DKRZ (SSP1-2.6 and SSP5-8.5): Deutsches Klimarechenzentrum, Hamburg 20146, Germany	SSP1-2.6 (Schupfner et al., 2019b) SSP5-8.5 (Schupfner et al., 2019a) historical (Jungclaus et al., 2019b) piControl (Jungclaus et al., 2019a)
UKESM1-0-LL	MOHC: Met Office Hadley Centre, Fitzroy Road, Exeter, Devon, EX1 3PB, UK	SSP1-2.6 (Good et al., 2019a) SSP5-8.5 (Good et al., 2019b) historical (Tang et al., 2019b) piControl (Tang et al., 2019a)
IPSL-CM6A-LR	IPSL: Institut Pierre Simon Laplace, Paris 75252, France	SSP1-2.6 (Boucher et al., 2019b) SSP5-8.5 (Boucher et al., 2019a) historical (Boucher et al., 2018b) piControl (Boucher et al., 2018a)
CanESM5	CCCma: Canadian Centre for Climate Modelling and Analysis, Environment and Climate Change Canada, Victoria, BC V8P 5C2, Canada	SSP1-2.6 (Swart et al., 2019d) SSP5-8.5 (Swart et al., 2019b) historical (Swart et al., 2019a) piControl (Swart et al., 2019c)
GFDL-ESM4	NOAA-GFDL: National Oceanic and Atmospheric Administration, Geophysical Fluid Dynamics Laboratory, Princeton, NJ 08540, USA	SSP1-2.6 (John et al., 2018a) SSP5-8.5 (John et al., 2018b) historical (Krasting et al., 2018b)

Appendix B Calculation of pO_2

pO_2 [mbar] at depth (Taylor, 1978; equation 5 rewritten; Bittig et al., 2018; Sect. E) can be written as a modified Henry's Law:

$$pO_2 = \frac{[O_2]}{K_0} \cdot \exp\left(\frac{V_m \cdot P}{R \cdot T}\right), \quad \text{(B1)}$$

with $K_0 = \frac{{O_2}^{sat}}{xO_2 \cdot (1013.25 - pH_2O)}$, and

$[O_2]$ as the insitu O_2 concentration (mol kg^{-1}), V_m the partial molar volume of O_2 ($31.7 \cdot 10^{-6}$ m^3 mol^{-1} (Enns et al., 1965)), P the approximated pressure (Pa; $P = 1025 \cdot 9.81 \cdot depth$ with depth in m), R the gas constant (8.3145 m^3·Pa·K^{-1}·mol^{-1}), T the absolute temperature (K), ${O_2}^{sat}$ the saturation O_2 concentration (mol kg^{-1}), xO_2 the dry air mole fraction of O_2 in air (0.20946; Glueckauf, 1951), and pH_2O the water vapor pressure (mbar).

The term $\exp\left(\frac{V_m \cdot P}{R \cdot T}\right)$ (unitless) is the pressure correction term for ${O_2}^{sat}$. We calculate the saturation concentration of O_2 in seawater (Garcia and Gordon, 1992) in mol kg^{-1} using Eq. B2.

$$O_2^{sat} = 10^{-6} * \exp(l) \text{ with} \quad \text{(B2)}$$

$$l = A_0 + A_1 * T_{scaled} + A_2 * {T_{scaled}}^2 + A_3 * {T_{scaled}}^3 + A_4 * {T_{scaled}}^4 + A_5 * {T_{scaled}}^5 + salinity * \left(B_0 + B_1 * T_{scaled} + B_2 * {T_{scaled}}^2 + B_3 * {T_{scaled}}^3\right) + C_0 * salinity^2,$$

where $T_{scaled} = \ln\left(\frac{298.15 - T_{insitu}}{KC + T_{insitu}}\right)$, KC=273.15 K and using salinity (psu) and insitu temperature Tinsitu (°C). The unitless constants $A_{0\text{-}5}$, $B_{0\text{-}3}$, and C_0 are listed in Table B1 (Benson and Krause, 1984; Garcia and Gordon, 1992; Sarmiento and Gruber, 2006).

Table B1 Constants for the calculation of O_2^{sat}

Constant	Value
A_0	5.80871
A_1	3.20291
A_2	4.17887
A_3	5.10006
A_4	-0.0986643
A_5	3.80369
B_0	-0.00701577
B_1	-0.00770028

B_2	-0.0113864
B_3	-0.00951519
C_0	-0.000000275915

We calculate the water vapor pressure pH_2O (mbar) following Weiss and Price (1980) (Eq. B3).

$$pH_2O = 1013.25 \cdot \exp\left(D_0 + D_1 \cdot \frac{100}{T_{insitu}+KC} + D_2 \cdot \ln\left(\frac{T_{insitu}+KC}{100}\right) + D_3 \cdot salinity\right), \quad \text{(A3)}$$

with D_0=24.4543, D_1=-67.4509, D_2=-4.8489, D_3=-5.44·10^{-4} .

Appendix C Additional figures

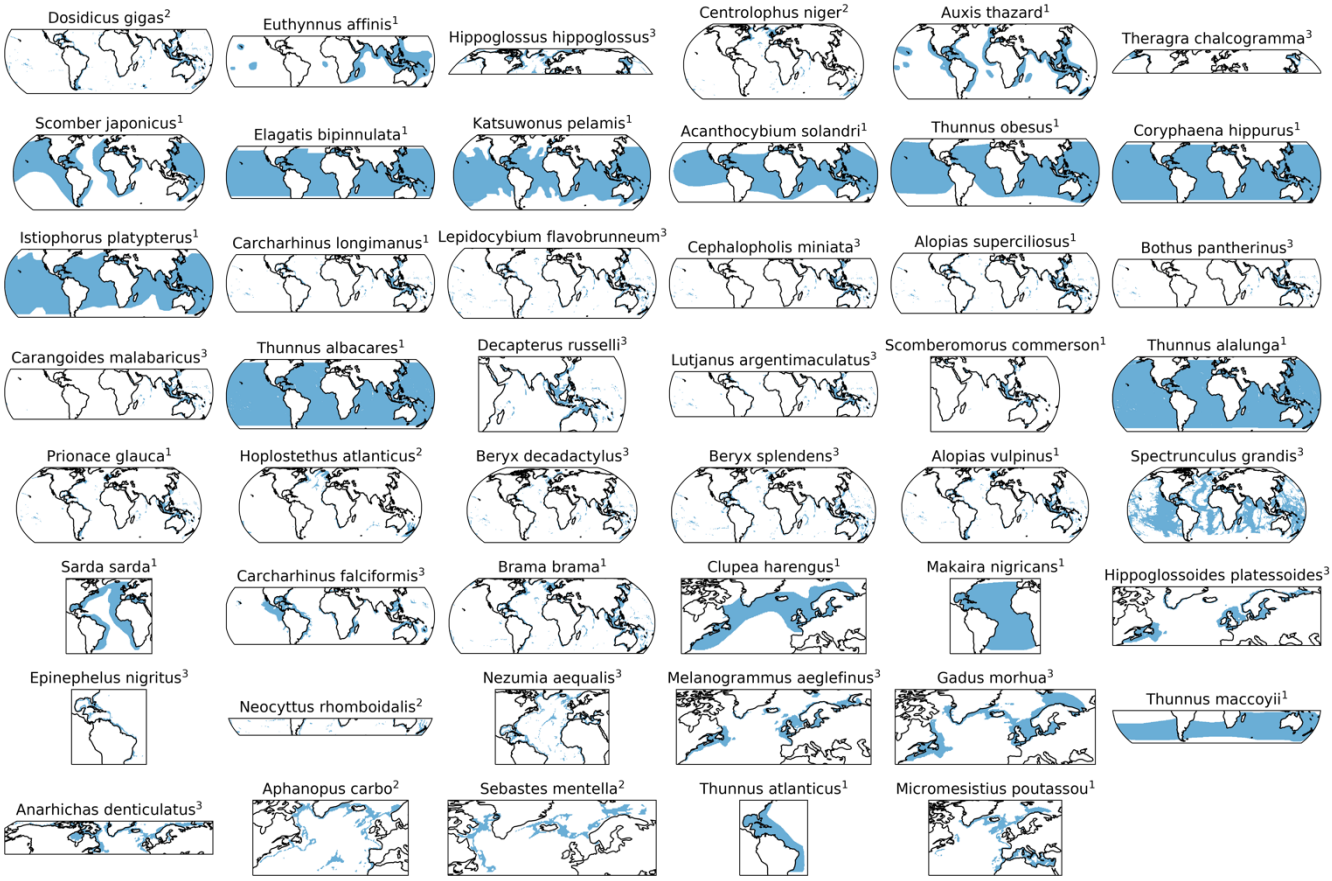

Figure C1 Horizontal distributions for each species in blue as based on Close et al. (2006), with superscript indicating the species' depth realm as in Table A1 (1=epipelagic, 2=mesopelagic, 3=demersal). Species are ordered based on the slope of the CDF (Fig. C9). These 2D habitats were extended over the depth range of the respective species' group for the analysis (Sect. 2.2).

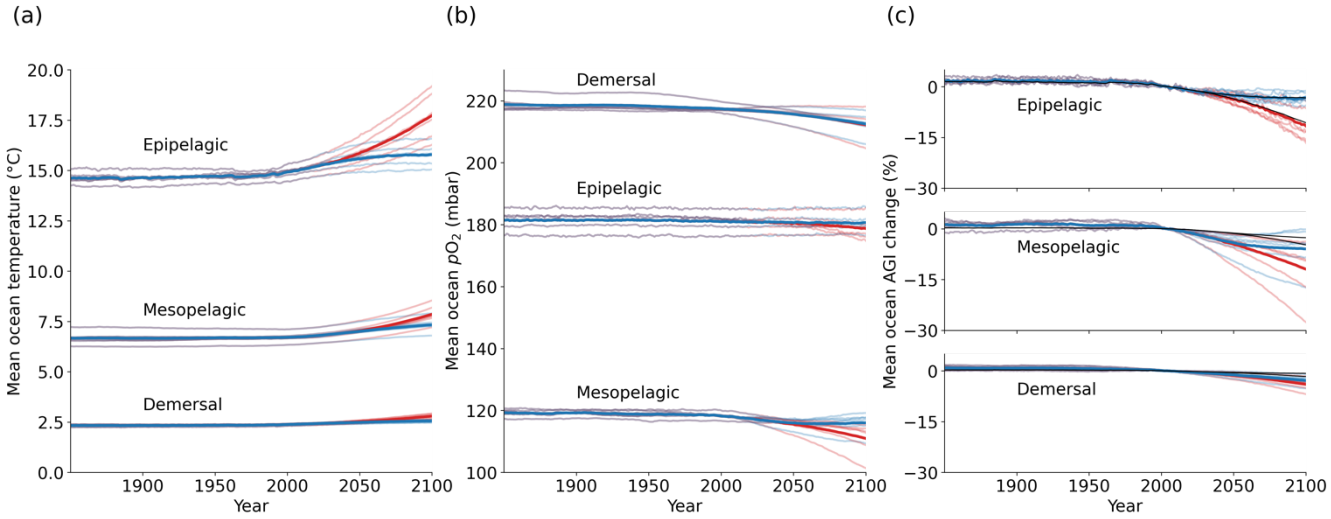

Figure C2 Global mean changes in ocean in-situ temperature in ºC (a), pO_2 in mbar (b) and AGI^{rel} in % (c) for years 1850-2100. The multi-model mean is given in opaque blue (SSP1-2.6) and red (SSP5-8.5). Individual models are shown in light blue and red without taking a running mean. AGI^{rel} is given relative to the 1995-2014 mean, and the mean contribution from temperature only (excluding the small effect of temperature on pO_2) is indicated by the black line in panel (c) and calculated by keeping pO_2 constant at its 1995-2014 mean state when calculating AGI^{rel}. AGI^{rel} is entirely species-independent (Eq. 2) and values that exceed 1000% or are below -1000% were excluded during the calculation of the global mean AGI changes to omit several grid-cells with extreme outliers caused by very small absolute changes in O_2 causing very large changes in AGI^{rel}.

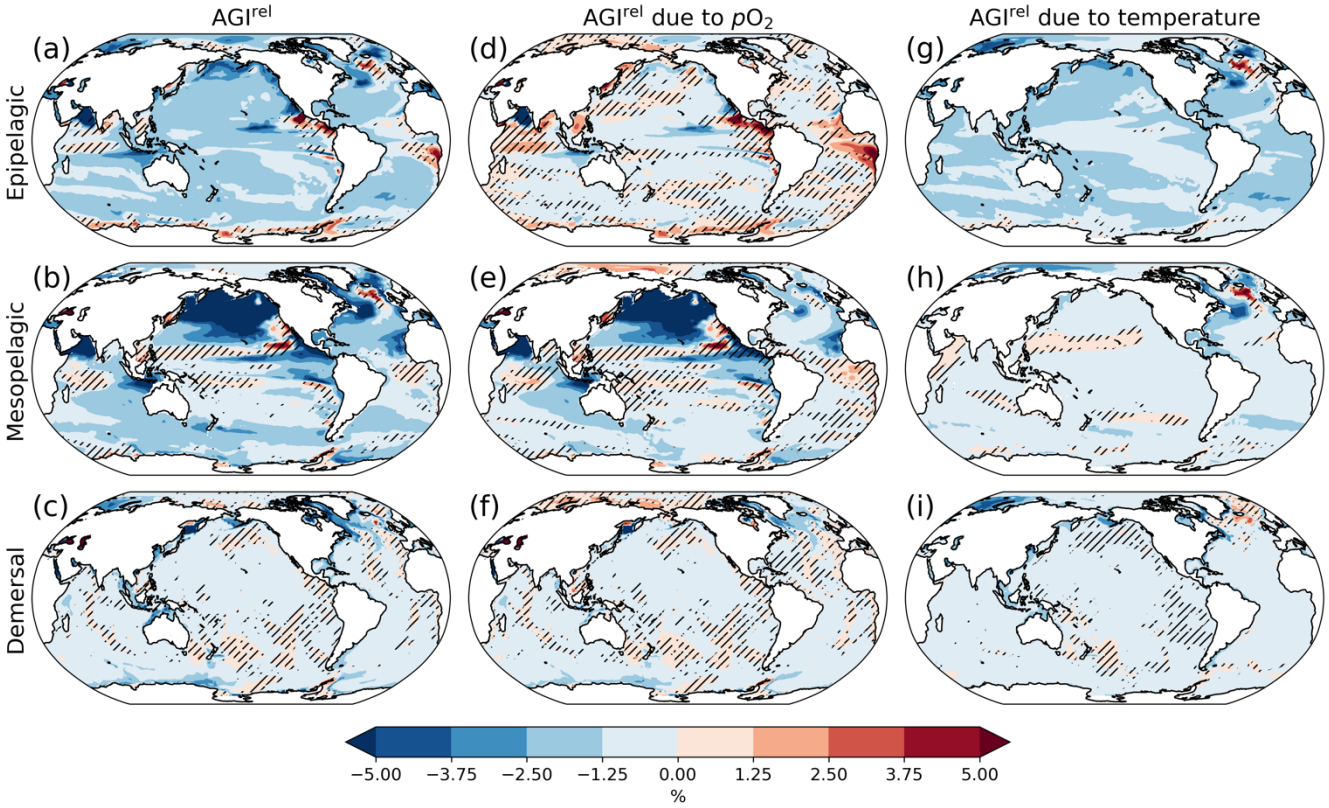

Figure C3 Multi-model mean AGI^{rel} relative to the 1995-2014 mean at 1.5 °C global warming (using the mean of the SSP1-2.6 and SSP5-8.5 simulations), vertically averaged over the epipelagic and mesopelagic realms, and shown for the demersal realm (a-c). AGI^{rel} is split up into the contribution from (d-f) pO_2 and (g-i) temperature. Data are hatched where the scenario mean of more than 2 out of the 6 models disagree about the sign of change. Note that sea floor depth and thus demersal depth depends strongly on location. Contributions from pO_2 (temperature) are calculated by keeping temperature (pO_2) constant at its 1995-2014 mean state when calculating AGI^{rel}. Further note that since $[O_2]$ depends on temperature too, the contribution to AGI^{rel} from pO_2 also contains a minor temperature component.

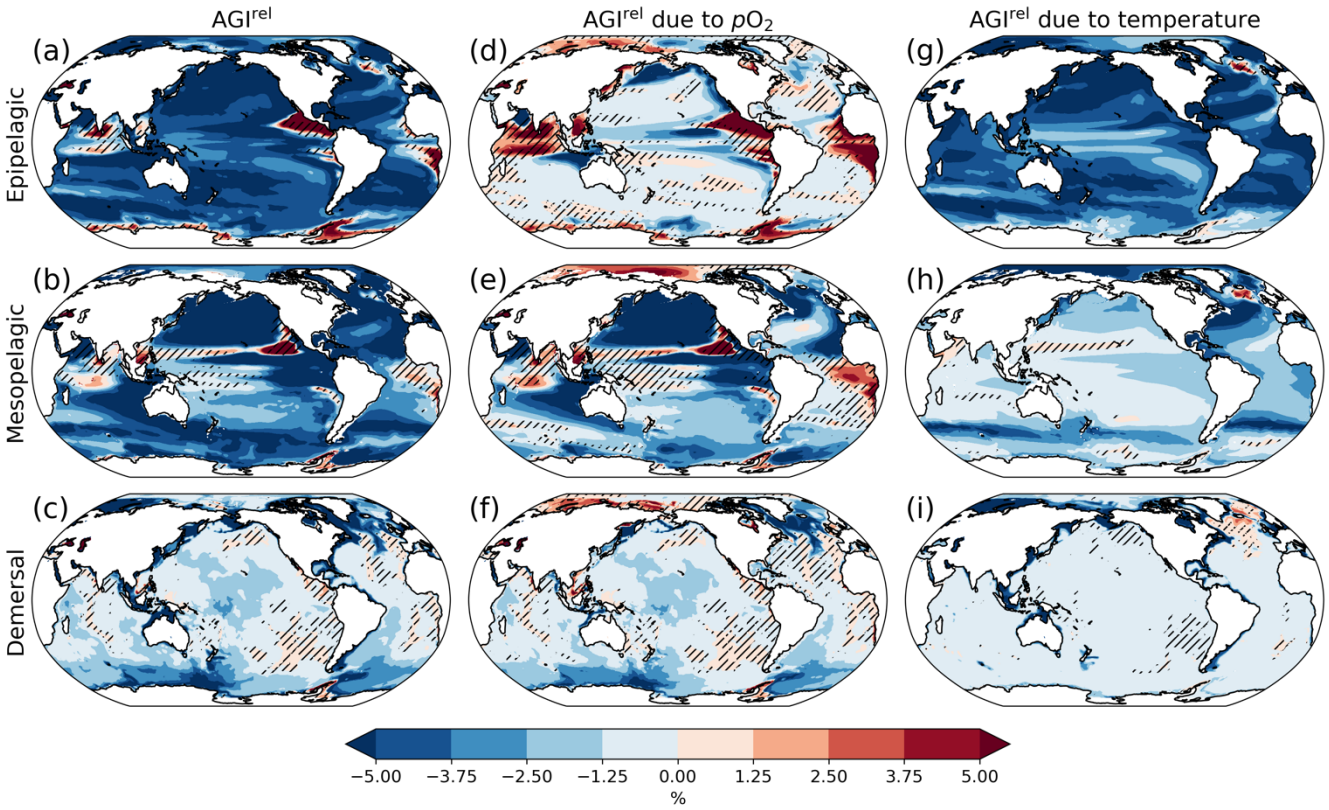

Figure C4 Same as Figure C3, but for 3°C global warming (and therefore using SSP5-8.5 simulations only).

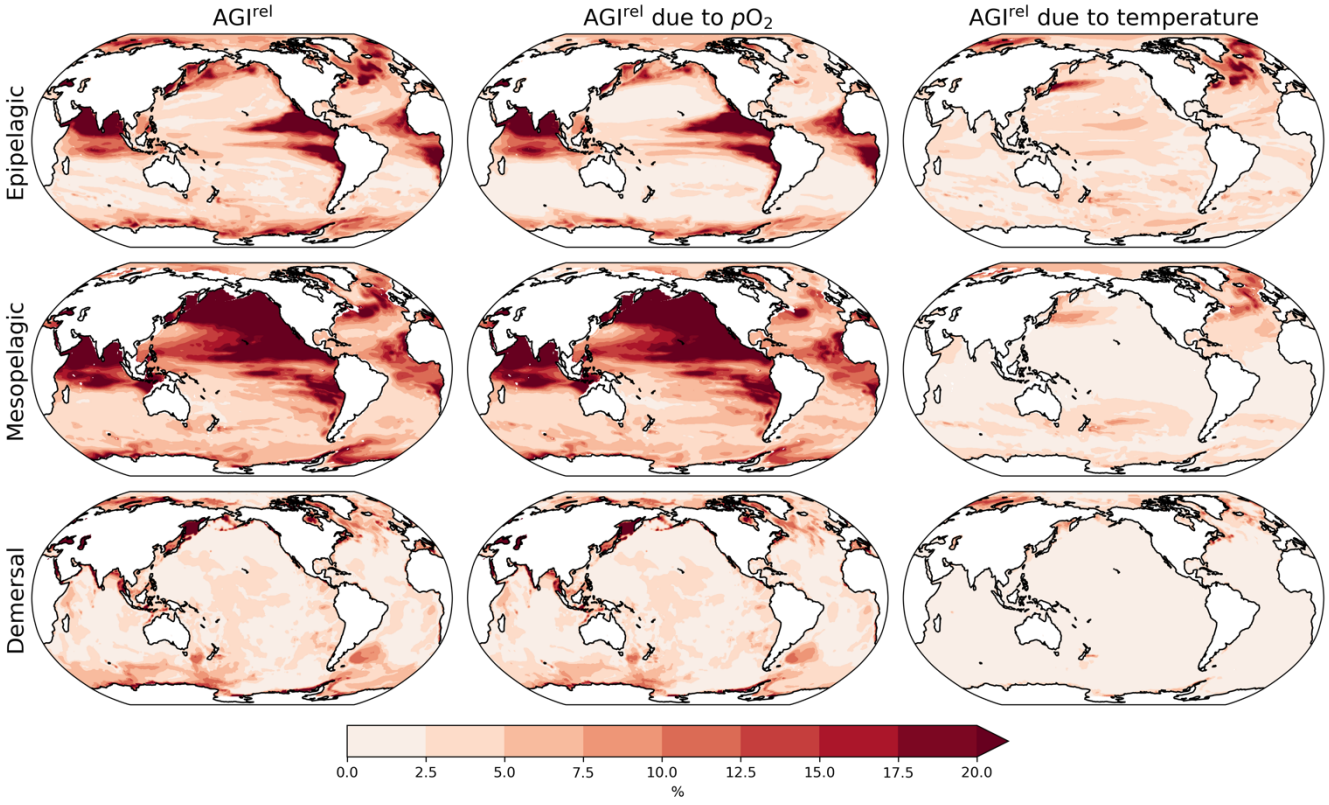

Figure C5 Multi-model range of AGI^{rel} at 2°C global warming for the three depth intervals studied.

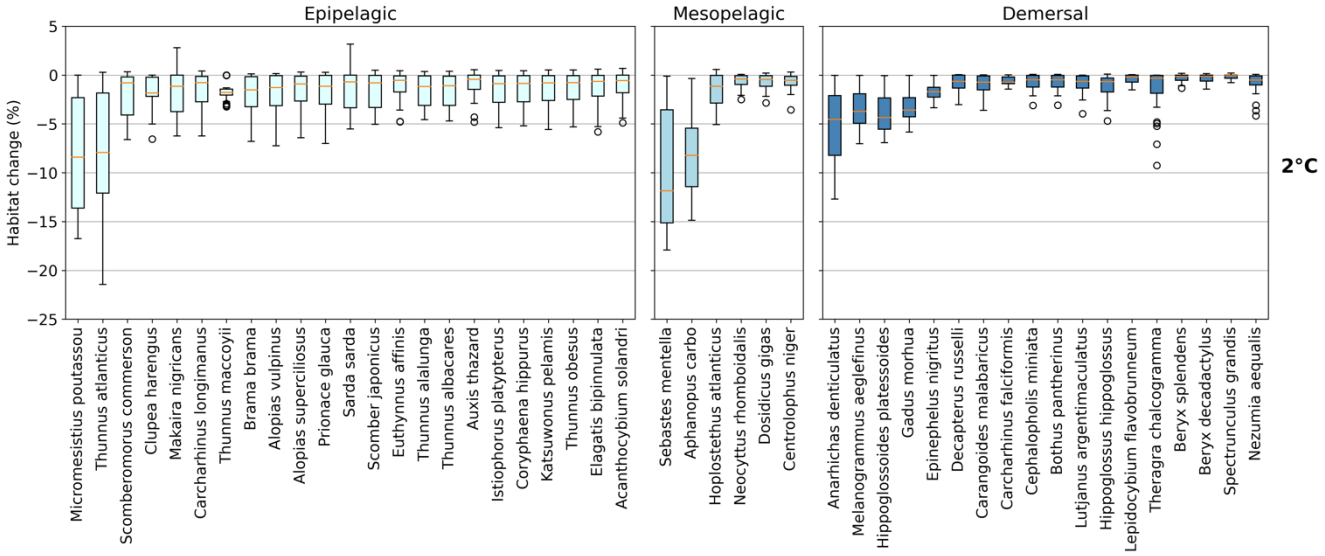

Figure C6 Habitat change (%) of contemporary (1995-2014) habitat volume for 2°C global warming, including 5 levels of AGI^{crit} in every species' boxplot (number of datapoints n=5 AGI^{crit} levels * 6 models = 30): AGI^{crit} is taken as the minimum in-habitat AGI value, the 5th percentile, the 10th percentile, the 15th percentile and the 20th percentile, respectively. Note the different y-axis when

comparing to Fig. 3. Each boxplot indicates the median in orange and a box bounded by the interquartile range (IQR; the 25th to 75th percentiles) and the whiskers extending to the data range with a maximum of 1.5×IQR, with outliers as open circles.

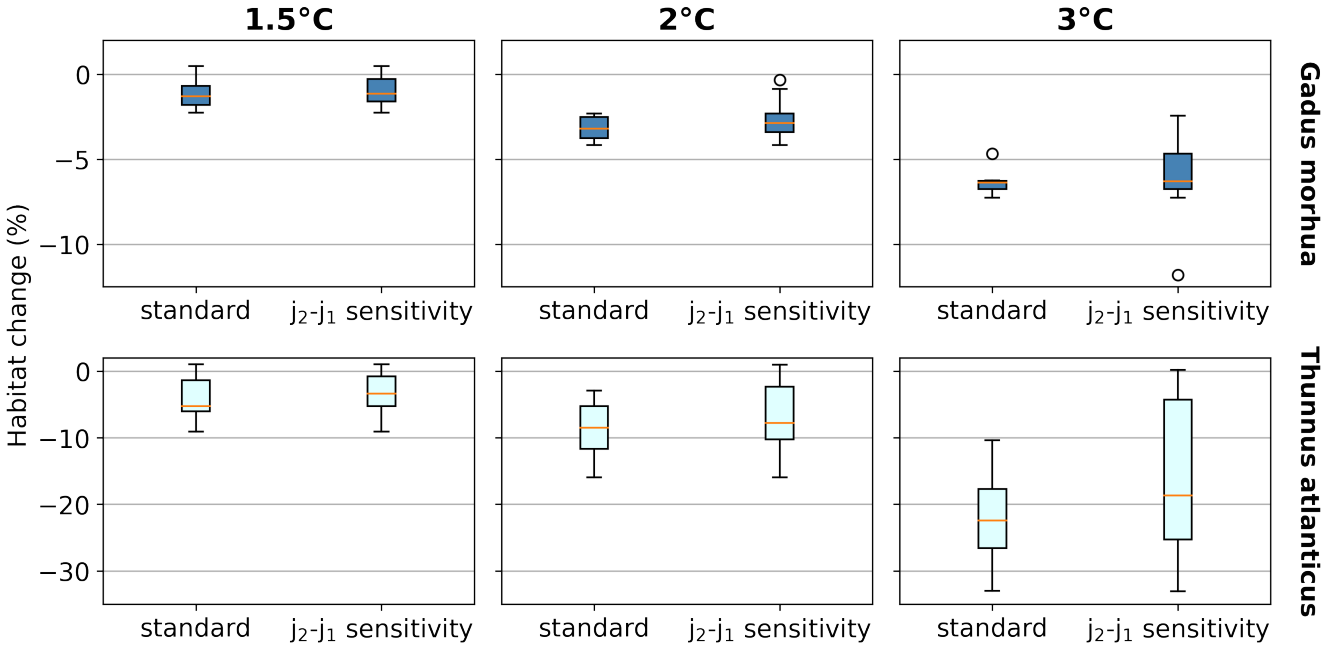

Figure C7 Habitat change (%) sensitivity to the choice of j_2-j_1 for the species *Gadus morhua* and *Thunnus atlanticus*. Standard results are as in Fig. 3 and use the standard j_2-j_1=3500K (Sect. 2.1). For 'j_2-j_1 sensitivity', j_2-j_1 is adjusted to represent low (high) temperature sensitivity of 1000K (6000K), which is equivalent to varying the standard j_2 and j_1 by ± 20% (resulting in the difference j_2-j_1 being varied by ± 71%), and recalculating AGI, AGI^{crit} and volume loss for each j_2-j_1. The standard, low and high j_2-j_1 are all included in the 'j_2-j_1 sensitivity' boxplots.

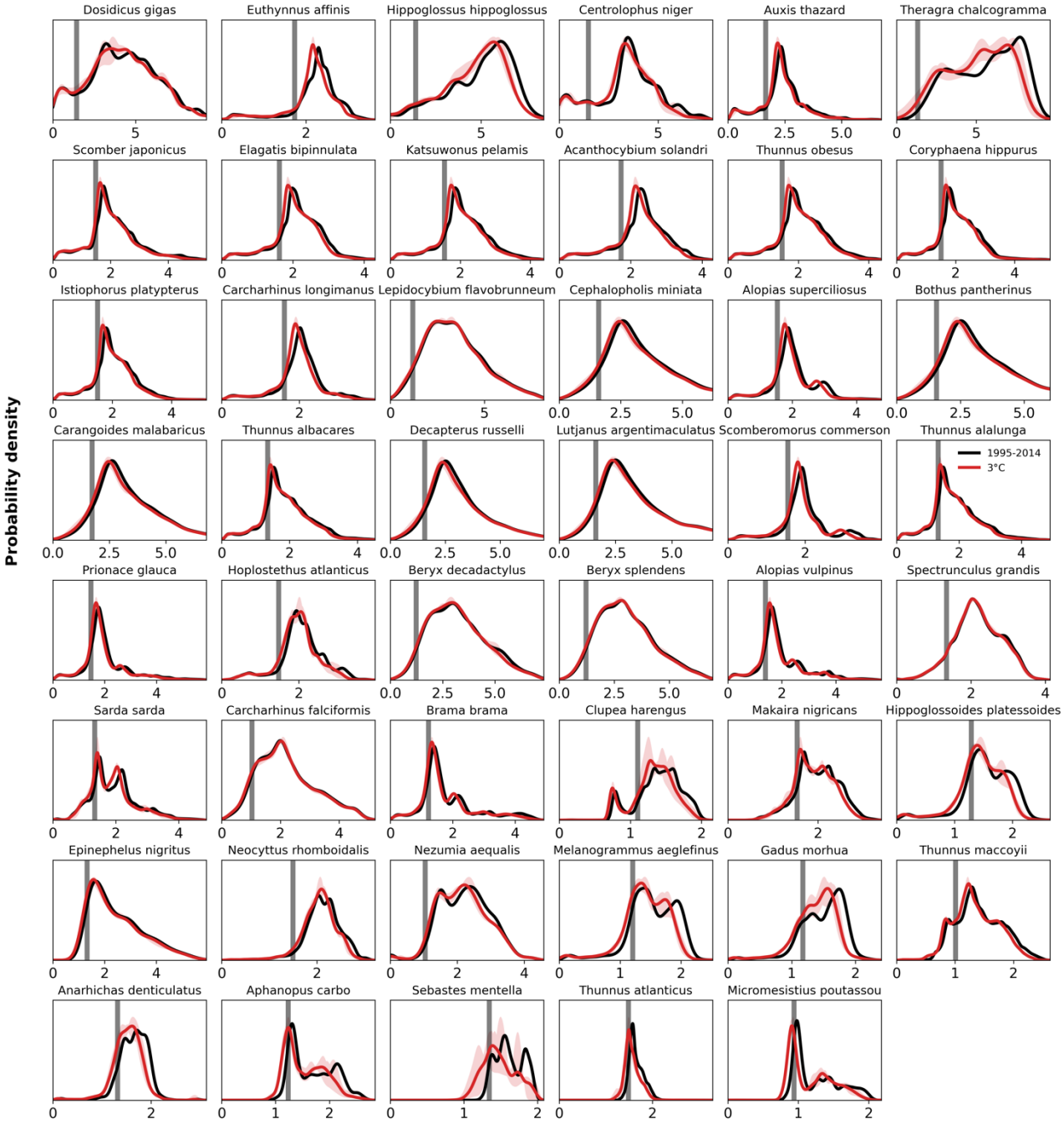

Figure C8 Probability density of AGI for each species for the contemporary reference period 1995-2014 (in black) and for 3°C global warming (in red with shaded model range). The PDF is a kernel-density estimate using Gaussian kernels, calculated using Python's SciPy package function 'gaussian_kde' with grid-cell volume taken as weights, following Scott's Rule, and evaluated at 50000 points from an AGI of 0 to 25. Species are ordered based on the slope of the CDF (Fig. C9).

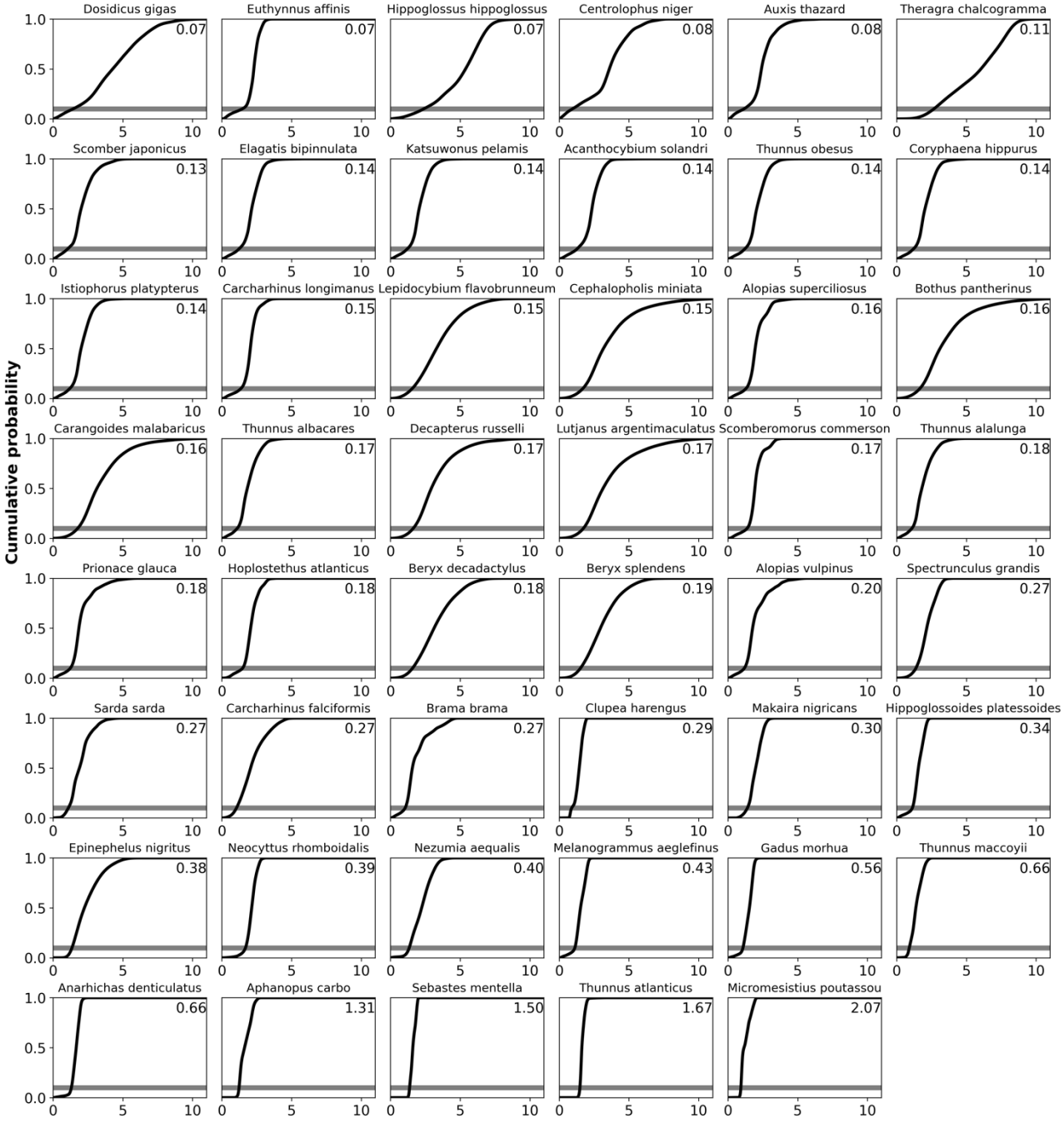

Figure C9 Cumulative density function of AGI at 1995-2014 for each species with "vulnerability" annotated in upper right corner (=slope at cumulative density of 0.1; i.e., at AGI=AGI^{crit}). The cumulative density is calculated as the cumulative sum of the probabilities in the PDF estimate (Fig. C8), normalized to a sum of 1. Species are ordered based on their slope.

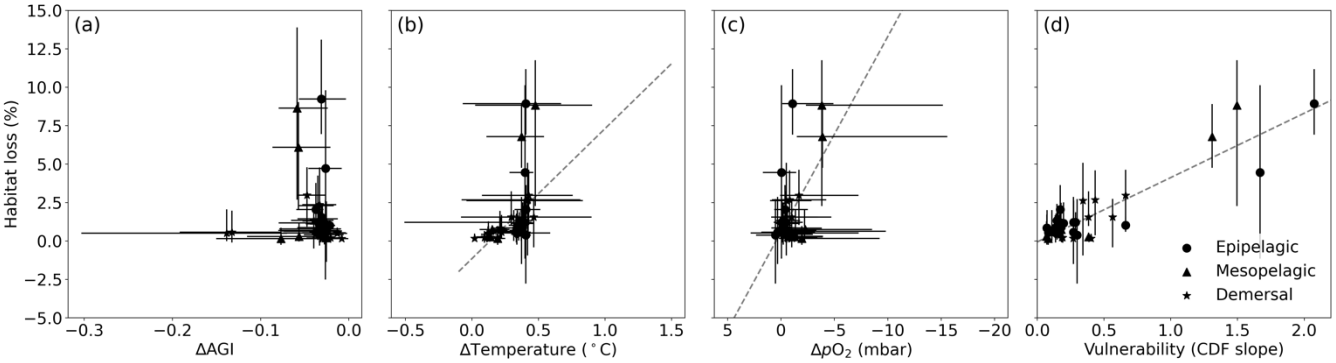

Figure C10 Multi-model mean in-habitat changes at 1.5°C of global warming of (a) AGI, (b) temperature, (c) pO_2 (mean over SSP1-2.6 and SSP5-8.5) and (d) vulnerability (CDF slope at a cumulative density of 0.1 based on 1995-2014 mean data, Fig. C9) plotted against loss of contemporary habitat volume for each species (model range indicated by error bars). There is no uncertainty in the vulnerability calculation because all models have the same 1995-2014 CDF slope due to the WOA18 bias-correction. From a linear regression to the data which is plotted in dashed grey we find an R^2 of 0.0% for (a) which line is therefore not plotted, 25% for (b), 27% for (c) and 85% for (d).

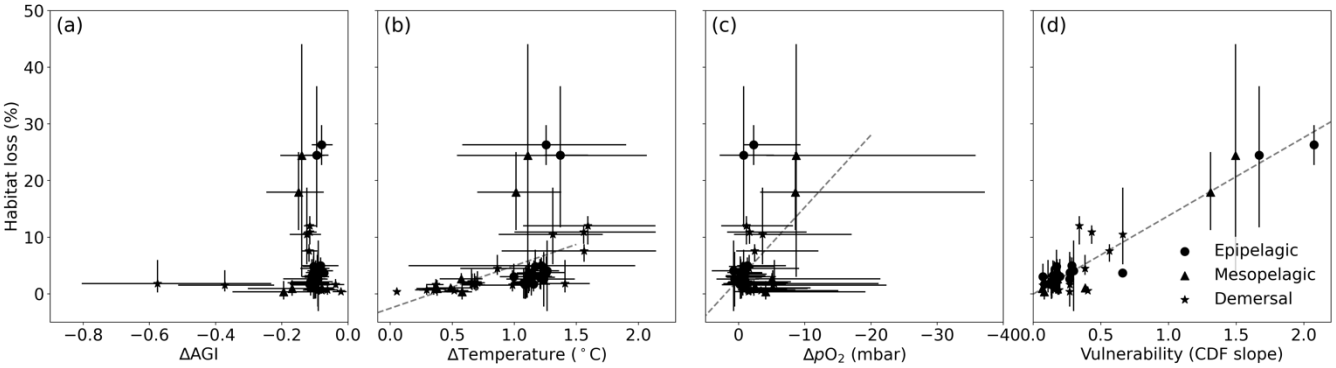

Figure C11 Same as Fig. C10, but for 3°C global warming (and therefore using SSP5-8.5 simulations only).

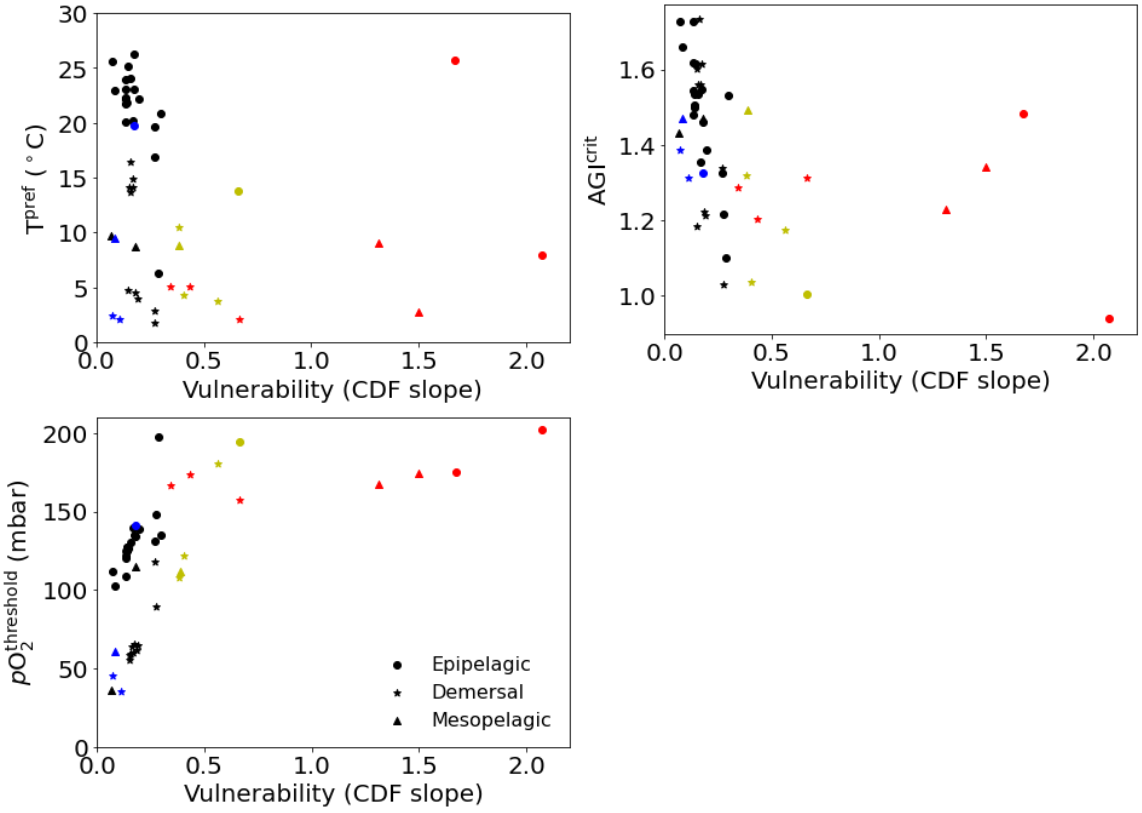

Figure C12 For each species T^{pref}, AGI^{crit} and $pO_2^{threshold}$ (see also Table A1) plotted against their vulnerability (=slope at cumulative density of 0.1; i.e., at AGI=AGI^{crit}; see also Fig. C9, Fig. 6, Table A1). Colors as in Fig. 6: For 2 °C global warming, species with > 5% loss marked in red, more than –0.1 ΔAGI in blue, and volume loss < 5% as well as vulnerability > 0.3 in yellow.

600

605

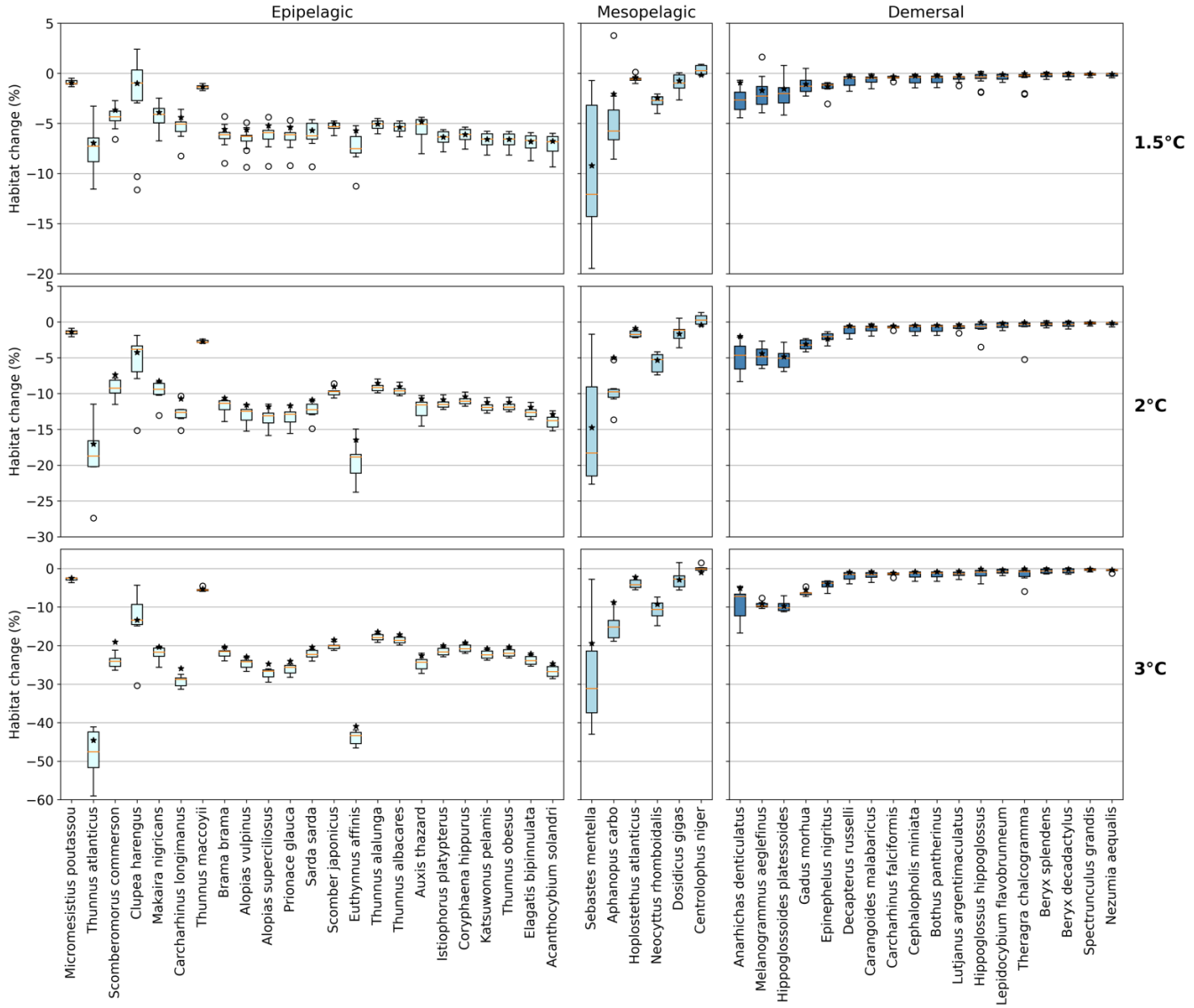

Figure C13 Habitat change (%) of contemporary (1995-2014) habitat volume for different levels of global warming, with negative values indicating habitat loss and positive values indicating habitat gain. This figure is the same as Fig. 3, but here applying surface values only in calculating $pO_2^{threshold}$, T^{pref} and AGI^{crit} and hence AGI and volume<AGI^{crit}. Demersal results are logically the same as in Fig. 3 as these consider only the sea floor. Note the different y-axes (also when comparing to Fig. 3). Each boxplot indicates the median in orange and a box bounded by the interquartile range (IQR; the 25th to 75th percentiles) and the whiskers extending to the data range with a maximum of 1.5×IQR, with outliers as open circles. As changes are expressed relative to the contemporary viable habitat volume (which is by definition 90% of the total habitat volume), values up to 10 % (=100-90) are possible.

Data availability

The CMIP6 model data are available at the Earth System Grid Federation (https://esgf-node.llnl.gov/search/cmip6; see Table A2 for references). The HadCRUT.5.0.1.0 data (retrieved 26th of April 2022) are taken from Morice et al. (2021). The species

habitat data are available at (DOI made upon publication of this manuscript). Scripts to make the figures will be shared on request to A. L. Morée.

Author contributions

All authors contributed to the conceptualization of the study. AM and TF collected the model data, while WC and TC provided species data. AM executed the formal analysis, investigation, and validation of the study with input from all co-authors. The extended version of AGI methodology was developed through discussion between all authors. AM wrote the initial draft and visualized the results with input from all co-authors.

Competing interests

The authors declare that they have no conflict of interest.

Acknowledgments

This study has been supported by the Swiss National Science Foundation under grant PP00P2_198897 and the European Union's Horizon 2020 research and innovation programme under grant agreement No 820989 (project COMFORT, Our common future ocean in the Earth system – quantifying coupled cycles of carbon, oxygen, and nutrients for determining and achieving safe operating spaces with respect to tipping points). We acknowledge the World Climate Research Programme, which, through its Working Group on Coupled Modelling, coordinated and promoted CMIP6. We thank the climate modelling groups for producing and making available their model output, the Earth System Grid Federation (ESGF) for archiving the data and providing access, and the multiple funding agencies who support CMIP6 and ESGF. The work reflects only the author's/authors' view; the European Commission and their executive agency are not responsible for any use that may be made of the information the work contains. We thank B. B. Cael for his suggestions for calculating the species' CDFs and Mridul K. Thomas for discussing the results with us. We thank the editor Mike Roman as well as two anonymous referees for their time to provide constructive feedback to our manuscript.

References

Andrews, O. D., Bindoff, N. L., Halloran, P. R., Ilyina, T., and Le Quéré, C.: Detecting an external influence on recent changes in oceanic oxygen using an optimal fingerprinting method, Biogeosciences, 10, 1799-1813, 10.5194/bg-10-1799-2013, 2013.

Baumann, H., Wallace, R. B., Tagliaferri, T., and Gobler, C. J.: Large Natural pH, CO2 and O2 Fluctuations in a Temperate Tidal Salt Marsh on Diel, Seasonal, and Interannual Time Scales, Estuaries and Coasts, 38, 220-231, 10.1007/s12237-014-9800-y, 2015.

Benson, B. B. and Krause, D.: The concentration and isotopic fractionation of oxygen dissolved in freshwater and seawater in equilibrium with the atmosphere, Limnology and Oceanography, 29, 620-632, https://doi.org/10.4319/lo.1984.29.3.0620, 1984.

Bindoff, N. L., Cheung, W. W. L., Kairo, J. G., Aristegui, J., Guinder, V. A., Hallberg, R., Hilmi, N., Jiao, N., Karim, M. s., Levin, L., O'Donoghue, S., Purca Cuicapusa, S. R., Rinkevich, B., Suga, T., Tagliabue, A., and Williamson, P.: Chapter 5: Changing Ocean, Marine Ecosystems, and Dependent Communities, IPCC Special Report on the Ocean and Cryosphere (SROCC), 2019.

Bittig, H., Körtzinger, A., Johnson, K., Claustre, H., Emerson, S., Fennel, K., Garcia, H., Gilbert, D., Gruber, N., Kang, D.-J., Naqvi, W., Prakash, S., Riser, S., Thierry, V., Tilbrook, B., Uchida, H., Ulloa, O., and Xing, X.: SCOR WG 142: Quality Control Procedures for Oxygen and Other Biogeochemical Sensors on Floats and Gliders. Recommendations on the conversion between oxygen quantities for Bio-Argo floats and other autonomous sensor platforms, Ifremer, 10.13155/45915, 2018.

Bopp, L., Resplandy, L., Orr, J. C., Doney, S. C., Dunne, J. P., Gehlen, M., Halloran, P., Heinze, C., Ilyina, T., Séférian, R., Tjiputra, J., and Vichi, M.: Multiple stressors of ocean ecosystems in the 21st century: projections with CMIP5 models, Biogeosciences, 10, 6225-6245, 10.5194/bg-10-6225-2013, 2013.

Boucher, O., Denvil, S., Levavasseur, G., Cozic, A., Caubel, A., Foujols, M.-A., Meurdesoif, Y., Cadule, P., Devilliers, M., Dupont, E., and Lurton, T.: IPSL IPSL-CM6A-LR model output prepared for CMIP6 ScenarioMIP ssp585, 10.22033/ESGF/CMIP6.5271, 2019a.

Boucher, O., Denvil, S., Levavasseur, G., Cozic, A., Caubel, A., Foujols, M.-A., Meurdesoif, Y., Cadule, P., Devilliers, M., Dupont, E., and Lurton, T.: IPSL IPSL-CM6A-LR model output prepared for CMIP6 ScenarioMIP ssp126, Earth System Grid Federation [dataset], 10.22033/ESGF/CMIP6.5262, 2019b.

Boucher, O., Denvil, S., Levavasseur, G., Cozic, A., Caubel, A., Foujols, M.-A., Meurdesoif, Y., Cadule, P., Devilliers, M., Ghattas, J., Lebas, N., Lurton, T., Mellul, L., Musat, I., Mignot, J., and Cheruy, F.: IPSL IPSL-CM6A-LR model output prepared for CMIP6 CMIP piControl, Earth System Grid Federation [dataset], 10.22033/ESGF/CMIP6.5251, 2018a.

Boucher, O., Denvil, S., Levavasseur, G., Cozic, A., Caubel, A., Foujols, M.-A., Meurdesoif, Y., Cadule, P., Devilliers, M., Ghattas, J., Lebas, N., Lurton, T., Mellul, L., Musat, I., Mignot, J., and Cheruy, F.: IPSL IPSL-CM6A-LR model output prepared for CMIP6 CMIP historical, 10.22033/ESGF/CMIP6.5195, 2018b.

Boyd, P. W., Collins, S., Dupont, S., Fabricius, K., Gattuso, J.-P., Havenhand, J., Hutchins, D. A., Riebesell, U., Rintoul, M. S., Vichi, M., Biswas, H., Ciotti, A., Gao, K., Gehlen, M., Hurd, C. L., Kurihara, H., McGraw, C. M., Navarro, J. M., Nilsson, G. E., Passow, U., and Pörtner, H.-O.: Experimental strategies to assess the biological ramifications of multiple drivers of global ocean change—A review, Global Change Biology, 24, 2239-2261, https://doi.org/10.1111/gcb.14102, 2018.

Boyer, T. P., Garcia, H. E., Locarnini, R. A., Zweng, M. M., Mishonov, A. V., Reagan, J. R., Weathers, K. W., Baranova, O. K., Seidov, D., and Smolyar, I. V.: World Ocean Atlas 2018 [oxygen, salinity and temperature] [dataset], 2018.

Breitburg, D., Levin, L. A., Oschlies, A., Grégoire, M., Chavez, F. P., Conley, D. J., Garçon, V., Gilbert, D., Gutiérrez, D., Isensee, K., Jacinto, G. S., Limburg, K. E., Montes, I., Naqvi, S. W. A., Pitcher, G. C., Rabalais, N. N., Roman, M. R., Rose, K. A., Seibel, B. A., Telszewski, M., Yasuhara, M., and Zhang, J.: Declining oxygen in the global ocean and coastal waters, Science, 359, eaam7240, doi:10.1126/science.aam7240, 2018.

Bryndum-Buchholz, A., Tittensor, D. P., Blanchard, J. L., Cheung, W. W. L., Coll, M., Galbraith, E. D., Jennings, S., Maury, O., and Lotze, H. K.: Twenty-first-century climate change impacts on marine animal biomass and ecosystem structure across ocean basins, Global Change Biology, 25, 459-472, https://doi.org/10.1111/gcb.14512, 2019.

Buchanan, P. J. and Tagliabue, A.: The Regional Importance of Oxygen Demand and Supply for Historical Ocean Oxygen Trends, Geophysical Research Letters, 48, e2021GL094797, https://doi.org/10.1029/2021GL094797, 2021.

Cabré, A., Marinov, I., Bernardello, R., and Bianchi, D.: Oxygen minimum zones in the tropical Pacific across CMIP5 models: mean state differences and climate change trends, Biogeosciences, 12, 5429-5454, 10.5194/bg-12-5429-2015, 2015.

Casanueva, A., Herrera, S., Iturbide, M., Lange, S., Jury, M., Dosio, A., Maraun, D., and Gutiérrez, J. M.: Testing bias adjustment methods for regional climate change applications under observational uncertainty and resolution mismatch, Atmospheric Science Letters, 21, e978, https://doi.org/10.1002/asl.978, 2020.

Cheung, W. W., Lam, V. W., and Pauly, D.: Dynamic bioclimate envelope model to predict climate-induced changes in distribution of marine fishes and invertebrates., 5-50, 2008.

Cheung, W. W. L., Reygondeau, G., and Frölicher, T. L.: Large benefits to marine fisheries of meeting the 1.5C global warming target, Science, 354, 1591-1594, doi:10.1126/science.aag2331, 2016.

Cheung, W. W. L., Dunne, J., Sarmiento, J. L., and Pauly, D.: Integrating ecophysiology and plankton dynamics into projected maximum fisheries catch potential under climate change in the Northeast Atlantic, ICES Journal of Marine Science, 68, 1008-1018, 10.1093/icesjms/fsr012, 2011.

Cheung, W. W. L., Lam, V. W. Y., Sarmiento, J. L., Kearney, K., Watson, R., and Pauly, D.: Projecting global marine biodiversity impacts under climate change scenarios, Fish and Fisheries, 10, 235-251, https://doi.org/10.1111/j.1467-2979.2008.00315.x, 2009.

CHEUNG, W. W. L., LAM, V. W. Y., SARMIENTO, J. L., KEARNEY, K., WATSON, R., ZELLER, D., and PAULY, D.: Large-scale redistribution of maximum fisheries catch potential in the global ocean under climate change, Global Change Biology, 16, 24-35, https://doi.org/10.1111/j.1365-2486.2009.01995.x, 2010.

Cheung, W. W. L., Frölicher, T. L., Lam, V. W. Y., Oyinlola, M. A., Reygondeau, G., Sumaila, U. R., Tai, T. C., Teh, L. C. L., and Wabnitz, C. C. C.: Marine high temperature extremes amplify the impacts of climate change on fish and fisheries, Science Advances, 7, eabh0895, 10.1126/sciadv.abh0895, 2021.

Clarke, T. M., Wabnitz, C. C. C., Striegel, S., Frölicher, T. L., Reygondeau, G., and Cheung, W. W. L.: Aerobic Growth Index (AGI): an index to understand the impacts of ocean warming and deoxygenation on global marine fisheries resources, Progress in Oceanography, 195, 102588, https://doi.org/10.1016/j.pocean.2021.102588, 2021.

Close, C., Cheung, W. L., Hodgson, S., Lam, V., Watson, R., and Pauly, D.: Distribution ranges of commercial fishes and invertebrates, in: Fishes in Databases and Ecosystems. Fisheries Centre Research Reports, Fisheries Centre, Univ. British Columbia, Vancouver, 2006.

Cocco, V., Joos, F., Steinacher, M., Frölicher, T. L., Bopp, L., Dunne, J., Gehlen, M., Heinze, C., Orr, J., Oschlies, A., Schneider, B., Segschneider, J., and Tjiputra, J.: Oxygen and indicators of stress for marine life in multi-model global warming projections, Biogeosciences, 10, 1849-1868, 10.5194/bg-10-1849-2013, 2013.

Collins, M., Truebano, M., Verberk, W. C. E. P., and Spicer, J. I.: Do aquatic ectotherms perform better under hypoxia after warm acclimation?, Journal of Experimental Biology, 224, 10.1242/jeb.232512, 2021.

Collins, S., Whittaker, H., and Thomas, M. K.: The need for unrealistic experiments in global change biology, Current Opinion in Microbiology, 68, 102151, https://doi.org/10.1016/j.mib.2022.102151, 2022.

Deser, C., Alexander, M. A., Xie, S.-P., and Phillips, A. S.: Sea Surface Temperature Variability: Patterns and Mechanisms, Annual Review of Marine Science, 2, 115-143, 10.1146/annurev-marine-120408-151453, 2009.

Deutsch, C., Penn, J. L., and Seibel, B.: Metabolic trait diversity shapes marine biogeography, Nature, 585, 557-562, 10.1038/s41586-020-2721-y, 2020.

Deutsch, C., Ferrel, A., Seibel, B., Pörtner, H.-O., and Huey, R. B.: Climate change tightens a metabolic constraint on marine habitats, Science, 348, 1132, 10.1126/science.aaa1605, 2015.

Doney, S. C., Ruckelshaus, M., Emmett Duffy, J., Barry, J. P., Chan, F., English, C. A., Galindo, H. M., Grebmeier, J. M., Hollowed, A. B., Knowlton, N., Polovina, J., Rabalais, N. N., Sydeman, W. J., and Talley, L. D.: Climate Change Impacts on Marine Ecosystems, Annual Review of Marine Science, 4, 11-37, 10.1146/annurev-marine-041911-111611, 2011.

Enns, T., Scholander, P. F., and Bradstreet, E. D.: Effect of Hydrostatic Pressure on Gases Dissolved in Water, The Journal of Physical Chemistry, 69, 389-391, 10.1021/j100886a005, 1965.

Eyring, V., Bony, S., Meehl, G. A., Senior, C. A., Stevens, B., Stouffer, R. J., and Taylor, K. E.: Overview of the Coupled Model Intercomparison Project Phase 6 (CMIP6) experimental design and organization, Geosci. Model Dev., 9, 1937-1958, 10.5194/gmd-9-1937-2016, 2016.

Fernandes, J. A., Cheung, W. W. L., Jennings, S., Butenschön, M., de Mora, L., Frölicher, T. L., Barange, M., and Grant, A.: Modelling the effects of climate change on the distribution and production of marine fishes: accounting for trophic interactions in a dynamic bioclimate envelope model, Global Change Biology, 19, 2596-2607, https://doi.org/10.1111/gcb.12231, 2013.

Frölicher, T. L. and Laufkötter, C.: Emerging risks from marine heat waves, Nature Communications, 9, 650, 10.1038/s41467-018-03163-6, 2018.

Frölicher, T. L., Joos, F., Plattner, G. K., Steinacher, M., and Doney, S. C.: Natural variability and anthropogenic trends in oceanic oxygen in a coupled carbon cycle–climate model ensemble, Global Biogeochemical Cycles, 23, https://doi.org/10.1029/2008GB003316, 2009.

Frölicher, T. L., Aschwanden, M. T., Gruber, N., Jaccard, S. L., Dunne, J. P., and Paynter, D.: Contrasting Upper and Deep Ocean Oxygen Response to Protracted Global Warming, Global Biogeochemical Cycles, 34, e2020GB006601, https://doi.org/10.1029/2020GB006601, 2020.

Garcia, H. E. and Gordon, L. I.: Oxygen solubility in seawater: Better fitting equations, Limnology and Oceanography, 37, 1307-1312, https://doi.org/10.4319/lo.1992.37.6.1307, 1992.
Garcia, H. E., Weathers, K. W., Paver, C. R., Smolyar, I. V., Boyer, T. P., Locarnini, R. A., Zweng, M. M., Mishonov, A. V., Baranova, O. K., Seidov, D., and Reagan, J. R.: World Ocean Atlas 2018, Volume 3: Dissolved Oxygen, Apparent Oxygen Utilization, and Dissolved Oxygen Saturation. A. Mishonov Technical Ed., NOAA Atlas NESDIS 83, 38 pp., 2019.
García-Molinos, J., Halpern, Benjamin S., Schoeman, David S., Brown, Christopher J., Kiessling, W., Moore, Pippa J., Pandolfi, John M., Poloczanska, Elvira S., Richardson, Anthony J., and Burrows, Michael T.: Climate velocity and the future global redistribution of marine biodiversity, Nature Climate Change, 6, 83-88, 10.1038/nclimate2769, 2016.
Glueckauf, E.: The Composition of Atmospheric Air, in: Compendium of Meteorology: Prepared under the Direction of the Committee on the Compendium of Meteorology, edited by: Byers, H. R., Landsberg, H. E., Wexler, H., Haurwitz, B., Spilhaus, A. F., Willett, H. C., Houghton, H. G., and Malone, T. F., American Meteorological Society, Boston, MA, 3-10, 10.1007/978-1-940033-70-9_1, 1951.
Good, P., Sellar, A., Tang, Y., Rumbold, S., Ellis, R., Kelley, D., and Kuhlbrodt, T.: MOHC UKESM1.0-LL model output prepared for CMIP6 ScenarioMIP ssp126, Earth System Grid Federation [dataset], 10.22033/ESGF/CMIP6.6333, 2019a.
Good, P., Sellar, A., Tang, Y., Rumbold, S., Ellis, R., Kelley, D., and Kuhlbrodt, T.: MOHC UKESM1.0-LL model output prepared for CMIP6 ScenarioMIP ssp585, 10.22033/ESGF/CMIP6.6405, 2019b.
Gotelli, N. J., Moyes, F., Antão, L. H., Blowes, S. A., Dornelas, M., McGill, B. J., Penny, A., Schipper, A. M., Shimadzu, H., Supp, S. R., Waldock, C. A., and Magurran, A. E.: Long-term changes in temperate marine fish assemblages are driven by a small subset of species, Global Change Biology, 28, 46-53, https://doi.org/10.1111/gcb.15947, 2021.
Grégoire, M., Garçon, V., Garcia, H., Breitburg, D., Isensee, K., Oschlies, A., Telszewski, M., Barth, A., Bittig, H. C., Carstensen, J., Carval, T., Chai, F., Chavez, F., Conley, D., Coppola, L., Crowe, S., Currie, K., Dai, M., Deflandre, B., Dewitte, B., Diaz, R., Garcia-Robledo, E., Gilbert, D., Giorgetti, A., Glud, R., Gutierrez, D., Hosoda, S., Ishii, M., Jacinto, G., Langdon, C., Lauvset, S. K., Levin, L. A., Limburg, K. E., Mehrtens, H., Montes, I., Naqvi, W., Paulmier, A., Pfeil, B., Pitcher, G., Pouliquen, S., Rabalais, N., Rabouille, C., Recape, V., Roman, M., Rose, K., Rudnick, D., Rummer, J., Schmechtig, C., Schmidtko, S., Seibel, B., Slomp, C., Sumalia, U. R., Tanhua, T., Thierry, V., Uchida, H., Wanninkhof, R., and Yasuhara, M.: A Global Ocean Oxygen Database and Atlas for Assessing and Predicting Deoxygenation and Ocean Health in the Open and Coastal Ocean, Frontiers in Marine Science, 8, 10.3389/fmars.2021.724913, 2021.
Gruber, N., Boyd, P. W., Frölicher, T. L., and Vogt, M.: Biogeochemical extremes and compound events in the ocean, Nature, 600, 395-407, 10.1038/s41586-021-03981-7, 2021.
Hausfather, Z., Marvel, K., Schmidt, G. A., Nielsen-Gammon, J. W., and Zelinka, M.: Climate simulations: recognize the 'hot model' problem, Nature, 605, 26-29, 10.1038/d41586-022-01192-2, 2022.
Hersbach, H., Bell, B., Berrisford, P., Hirahara, S., Horányi, A., Muñoz-Sabater, J., Nicolas, J., Peubey, C., Radu, R., Schepers, D., Simmons, A., Soci, C., Abdalla, S., Abellan, X., Balsamo, G., Bechtold, P., Biavati, G., Bidlot, J., Bonavita, M., De Chiara, G., Dahlgren, P., Dee, D., Diamantakis, M., Dragani, R., Flemming, J., Forbes, R., Fuentes, M., Geer, A., Haimberger, L., Healy, S., Hogan, R. J., Hólm, E., Janisková, M., Keeley, S., Laloyaux, P., Lopez, P., Lupu, C., Radnoti, G., de Rosnay, P., Rozum, I., Vamborg, F., Villaume, S., and Thépaut, J.-N.: The ERA5 global reanalysis, Quarterly Journal of the Royal Meteorological Society, 146, 1999-2049, https://doi.org/10.1002/qj.3803, 2020.
IPCC: Summary for Policymakers. In: IPCC Special Report on the Ocean and Cryosphere in a Changing Climate 2019.
IPCC: Climate Change 2021: The Physical Science Basis. Contribution of Working Group I to the Sixth Assessment Report of the Intergovernmental Panel on Climate Change, Cambridge University Press, Cambridge, United Kingdom and New York, NY, USA, 10.1017/9781009157896, 2021.
Ito, T., Minobe, S., Long, M. C., and Deutsch, C.: Upper ocean O2 trends: 1958–2015, Geophysical Research Letters, 44, 4214-4223, https://doi.org/10.1002/2017GL073613, 2017.
Jacox, M. G., Alexander, M. A., Bograd, S. J., and Scott, J. D.: Thermal displacement by marine heatwaves, Nature, 584, 82-86, 10.1038/s41586-020-2534-z, 2020.
John, J. G., Blanton, C., McHugh, C., Radhakrishnan, A., Rand, K., Vahlenkamp, H., Wilson, C., Zadeh, N. T., Dunne, J. P., Dussin, R., Horowitz, L. W., Krasting, J. P., Lin, P., Malyshev, S., Naik, V., Ploshay, J., Shevliakova, E., Silvers, L., Stock, C., Winton, M., and Zeng, Y.: NOAA-GFDL GFDL-ESM4 model output prepared for CMIP6 ScenarioMIP ssp126, Earth System Grid Federation [dataset], 10.22033/ESGF/CMIP6.8684, 2018a.

John, J. G., Blanton, C., McHugh, C., Radhakrishnan, A., Rand, K., Vahlenkamp, H., Wilson, C., Zadeh, N. T., Dunne, J. P., Dussin, R., Horowitz, L. W., Krasting, J. P., Lin, P., Malyshev, S., Naik, V., Ploshay, J., Shevliakova, E., Silvers, L., Stock, C., Winton, M., and Zeng, Y.: NOAA-GFDL GFDL-ESM4 model output prepared for CMIP6 ScenarioMIP ssp585, 10.22033/ESGF/CMIP6.8706, 2018b.

Jungclaus, J., Bittner, M., Wieners, K.-H., Wachsmann, F., Schupfner, M., Legutke, S., Giorgetta, M., Reick, C., Gayler, V., Haak, H., de Vrese, P., Raddatz, T., Esch, M., Mauritsen, T., von Storch, J.-S., Behrens, J., Brovkin, V., Claussen, M., Crueger, T., Fast, I., Fiedler, S., Hagemann, S., Hohenegger, C., Jahns, T., Kloster, S., Kinne, S., Lasslop, G., Kornblueh, L., Marotzke, J., Matei, D., Meraner, K., Mikolajewicz, U., Modali, K., Müller, W., Nabel, J., Notz, D., Peters-von Gehlen, K., Pincus, R., Pohlmann, H., Pongratz, J., Rast, S., Schmidt, H., Schnur, R., Schulzweida, U., Six, K., Stevens, B., Voigt, A., and Roeckner, E.: MPI-M MPI-ESM1.2-HR model output prepared for CMIP6 CMIP piControl, 10.22033/ESGF/CMIP6.6674, 2019a.

Jungclaus, J., Bittner, M., Wieners, K.-H., Wachsmann, F., Schupfner, M., Legutke, S., Giorgetta, M., Reick, C., Gayler, V., Haak, H., de Vrese, P., Raddatz, T., Esch, M., Mauritsen, T., von Storch, J.-S., Behrens, J., Brovkin, V., Claussen, M., Crueger, T., Fast, I., Fiedler, S., Hagemann, S., Hohenegger, C., Jahns, T., Kloster, S., Kinne, S., Lasslop, G., Kornblueh, L., Marotzke, J., Matei, D., Meraner, K., Mikolajewicz, U., Modali, K., Müller, W., Nabel, J., Notz, D., Peters-von Gehlen, K., Pincus, R., Pohlmann, H., Pongratz, J., Rast, S., Schmidt, H., Schnur, R., Schulzweida, U., Six, K., Stevens, B., Voigt, A., and Roeckner, E.: MPI-M MPI-ESM1.2-HR model output prepared for CMIP6 CMIP historical, 10.22033/ESGF/CMIP6.6594, 2019b.

Keeling, R. F., Körtzinger, A., and Gruber, N.: Ocean Deoxygenation in a Warming World, Annual Review of Marine Science, 2, 199-229, 10.1146/annurev.marine.010908.163855, 2010.

Krasting, J. P., John, J. G., Blanton, C., McHugh, C., Nikonov, S., Radhakrishnan, A., Rand, K., Zadeh, N. T., Balaji, V., Durachta, J., Dupuis, C., Menzel, R., Robinson, T., Underwood, S., Vahlenkamp, H., Dunne, K. A., Gauthier, P. P. G., Ginoux, P., Griffies, S. M., Hallberg, R., Harrison, M., Hurlin, W., Malyshev, S., Naik, V., Paulot, F., Paynter, D. J., Ploshay, J., Reichl, B. G., Schwarzkopf, D. M., Seman, C. J., Silvers, L., Wyman, B., Zeng, Y., Adcroft, A., Dunne, J. P., Dussin, R., Guo, H., He, J., Held, I. M., Horowitz, L. W., Lin, P., Milly, P. C. D., Shevliakova, E., Stock, C., Winton, M., Wittenberg, A. T., Xie, Y., and Zhao, M.: NOAA-GFDL GFDL-ESM4 model output prepared for CMIP6 CMIP piControl, Earth System Grid Federation [dataset], 10.22033/ESGF/CMIP6.8669, 2018a.

Krasting, J. P., John, J. G., Blanton, C., McHugh, C., Nikonov, S., Radhakrishnan, A., Rand, K., Zadeh, N. T., Balaji, V., Durachta, J., Dupuis, C., Menzel, R., Robinson, T., Underwood, S., Vahlenkamp, H., Dunne, K. A., Gauthier, P. P. G., Ginoux, P., Griffies, S. M., Hallberg, R., Harrison, M., Hurlin, W., Malyshev, S., Naik, V., Paulot, F., Paynter, D. J., Ploshay, J., Reichl, B. G., Schwarzkopf, D. M., Seman, C. J., Silvers, L., Wyman, B., Zeng, Y., Adcroft, A., Dunne, J. P., Dussin, R., Guo, H., He, J., Held, I. M., Horowitz, L. W., Lin, P., Milly, P. C. D., Shevliakova, E., Stock, C., Winton, M., Wittenberg, A. T., Xie, Y., and Zhao, M.: NOAA-GFDL GFDL-ESM4 model output prepared for CMIP6 CMIP historical, 10.22033/ESGF/CMIP6.8597, 2018b.

Kwiatkowski, L., Torres, O., Bopp, L., Aumont, O., Chamberlain, M., Christian, J. R., Dunne, J. P., Gehlen, M., Ilyina, T., John, J. G., Lenton, A., Li, H., Lovenduski, N. S., Orr, J. C., Palmieri, J., Santana-Falcón, Y., Schwinger, J., Séférian, R., Stock, C. A., Tagliabue, A., Takano, Y., Tjiputra, J., Toyama, K., Tsujino, H., Watanabe, M., Yamamoto, A., Yool, A., and Ziehn, T.: Twenty-first century ocean warming, acidification, deoxygenation, and upper-ocean nutrient and primary production decline from CMIP6 model projections, Biogeosciences, 17, 3439-3470, 10.5194/bg-17-3439-2020, 2020.

Levin, L. A. and Le Bris, N.: The deep ocean under climate change, Science, 350, 766-768, doi:10.1126/science.aad0126, 2015.

Liao, M.-l., Li, G.-y., Wang, J., Marshall, D. J., Hui, T. Y., Ma, S.-y., Zhang, Y.-m., Helmuth, B., and Dong, Y.-w.: Physiological determinants of biogeography: The importance of metabolic depression to heat tolerance, Global Change Biology, 27, 2561-2579, https://doi.org/10.1111/gcb.15578, 2021.

Locarnini, R. A., Mishonov, A. V., Baranova, O. K., Boyer, T. P., Zweng, M. M., Garcia, H. E., Reagan, J. R., Seidov, D., Weathers, K. W., Paver, C. R., and Smolyar, I. V.: World Ocean Atlas 2018, Volume 1: Temperature. A. Mishonov Technical Ed., NOAA Atlas NESDIS 81, 52 pp., 2019.

Long, M. C., Deutsch, C., and Ito, T.: Finding forced trends in oceanic oxygen, Global Biogeochemical Cycles, 30, 381-397, https://doi.org/10.1002/2015GB005310, 2016.

Maraun, D.: Bias Correcting Climate Change Simulations - a Critical Review, Current Climate Change Reports, 2, 211-220, 10.1007/s40641-016-0050-x, 2016.

McCormick, L. R. and Levin, L. A.: Physiological and ecological implications of ocean deoxygenation for vision in marine organisms, Philosophical Transactions of the Royal Society A: Mathematical, Physical and Engineering Sciences, 375, 20160322, 10.1098/rsta.2016.0322, 2017.

Meehl, G. A., Senior, C. A., Eyring, V., Flato, G., Lamarque, J.-F., Stouffer, R. J., Taylor, K. E., and Schlund, M.: Context for interpreting equilibrium climate sensitivity and transient climate response from the CMIP6 Earth system models, Science Advances, 6, 10.1126/sciadv.aba1981, 2020.

Meinshausen, M., Lewis, J., McGlade, C., Gütschow, J., Nicholls, Z., Burdon, R., Cozzi, L., and Hackmann, B.: Realization of Paris Agreement pledges may limit warming just below 2 °C, Nature, 604, 304-309, 10.1038/s41586-022-04553-z, 2022.

Morice, C. P., Kennedy, J. J., Rayner, N. A., Winn, J. P., Hogan, E., Killick, R. E., Dunn, R. J. H., Osborn, T. J., Jones, P. D., and Simpson, I. R.: An Updated Assessment of Near-Surface Temperature Change From 1850: The HadCRUT5 Data Set, Journal of Geophysical Research: Atmospheres, 126, e2019JD032361, https://doi.org/10.1029/2019JD032361, 2021.

Oschlies, A.: A committed fourfold increase in ocean oxygen loss, Nature Communications, 12, 2307, 10.1038/s41467-021-22584-4, 2021.

Oschlies, A., Brandt, P., Stramma, L., and Schmidtko, S.: Drivers and mechanisms of ocean deoxygenation, Nature Geoscience, 11, 467-473, 10.1038/s41561-018-0152-2, 2018.

Oschlies, A., Duteil, O., Getzlaff, J., Koeve, W., Landolfi, A., and Schmidtko, S.: Patterns of deoxygenation: sensitivity to natural and anthropogenic drivers, Philosophical Transactions of the Royal Society A: Mathematical, Physical and Engineering Sciences, 375, 20160325, doi:10.1098/rsta.2016.0325, 2017.

Palumbi, S. R., Evans, T. G., Pespeni, M. H., and Somero, G. N.: Present and future adaptation of marine species assemblages: DNA-based insights into climate change from studies of physiology, genomics, and evolution, Oceanography, 32, 82-93, https://doi.org/10.5670/oceanog.2019.314, 2019.

Pauly, D.: Gasping fish and panting squids: oxygen, temperature and the growth of water-breathing animals. International Ecology Institute.,

Pauly, D. and Cheung, W. W. L.: Sound physiological knowledge and principles in modeling shrinking of fishes under climate change, Global Change Biology, 24, e15-e26, https://doi.org/10.1111/gcb.13831, 2018.

Penn, J. L., Deutsch, C., Payne, J. L., and Sperling, E. A.: Temperature-dependent hypoxia explains biogeography and severity of end-Permian marine mass extinction, Science, 362, eaat1327, doi:10.1126/science.aat1327, 2018.

Perry, A. L., Low, P. J., Ellis, J. R., and Reynolds, J. D.: Climate Change and Distribution Shifts in Marine Fishes, Science, 308, 1912-1915, doi:10.1126/science.1111322, 2005.

Pinsky, M. L., Worm, B., Fogarty, M. J., Sarmiento, J. L., and Levin, S. A.: Marine Taxa Track Local Climate Velocities, Science, 341, 1239-1242, 10.1126/science.1239352, 2013.

Pitcher, G. C., Aguirre-Velarde, A., Breitburg, D., Cardich, J., Carstensen, J., Conley, D. J., Dewitte, B., Engel, A., Espinoza-Morriberón, D., Flores, G., Garçon, V., Graco, M., Grégoire, M., Gutiérrez, D., Hernandez-Ayon, J. M., Huang, H.-H. M., Isensee, K., Jacinto, M. E., Levin, L., Lorenzo, A., Machu, E., Merma, L., Montes, I., Swa, N., Paulmier, A., Roman, M., Rose, K., Hood, R., Rabalais, N. N., Salvanes, A. G. V., Salvatteci, R., Sánchez, S., Sifeddine, A., Tall, A. W., Plas, A. K. v. d., Yasuhara, M., Zhang, J., and Zhu, Z. Y.: System controls of coastal and open ocean oxygen depletion, Progress in Oceanography, 197, 102613, https://doi.org/10.1016/j.pocean.2021.102613, 2021.

Poloczanska, E. S., Burrows, M. T., Brown, C. J., García Molinos, J., Halpern, B. S., Hoegh-Guldberg, O., Kappel, C. V., Moore, P. J., Richardson, A. J., Schoeman, D. S., and Sydeman, W. J.: Responses of Marine Organisms to Climate Change across Oceans, Frontiers in Marine Science, 3, 10.3389/fmars.2016.00062, 2016.

Poloczanska, E. S., Brown, C. J., Sydeman, W. J., Kiessling, W., Schoeman, D. S., Moore, P. J., Brander, K., Bruno, J. F., Buckley, L. B., Burrows, M. T., Duarte, C. M., Halpern, B. S., Holding, J., Kappel, C. V., O'Connor, M. I., Pandolfi, J. M., Parmesan, C., Schwing, F., Thompson, S. A., and Richardson, A. J.: Global imprint of climate change on marine life, Nature Climate Change, 3, 919-925, 10.1038/nclimate1958, 2013.

Pörtner, H. O.: Oxygen- and capacity-limitation of thermal tolerance: a matrix for integrating climate-related stressor effects in marine ecosystems, Journal of Experimental Biology, 213, 881-893, 10.1242/jeb.037523, 2010.

Pörtner, H. O. and Knust, R.: Climate Change Affects Marine Fishes Through the Oxygen Limitation of Thermal Tolerance, Science, 315, 95-97, doi:10.1126/science.1135471, 2007.

Pörtner, H. O. and Peck, M. A.: TEMPERATURE | Effects of Climate Change, in: Encyclopedia of Fish Physiology, edited by: Farrell, A. P., Academic Press, San Diego, 1738-1745, https://doi.org/10.1016/B978-0-12-374553-8.00197-0, 2011.

Sampaio, E., Santos, C., Rosa, I. C., Ferreira, V., Pörtner, H.-O., Duarte, C. M., Levin, L. A., and Rosa, R.: Impacts of hypoxic events surpass those of future ocean warming and acidification, Nature Ecology & Evolution, 5, 311-321, 10.1038/s41559-020-01370-3, 2021.

Sarmiento, J. L. and Gruber, N.: Ocean Biogeochemical Dynamics, Princeton University Press, 2006.

Schmidtko, S., Stramma, L., and Visbeck, M.: Decline in global oceanic oxygen content during the past five decades, Nature, 542, 335-339, 10.1038/nature21399, 2017.

Schupfner, M., Wieners, K.-H., Wachsmann, F., Steger, C., Bittner, M., Jungclaus, J., Früh, B., Pankatz, K., Giorgetta, M., Reick, C., Legutke, S., Esch, M., Gayler, V., Haak, H., de Vrese, P., Raddatz, T., Mauritsen, T., von Storch, J.-S., Behrens, J., Brovkin, V., Claussen, M., Crueger, T., Fast, I., Fiedler, S., Hagemann, S., Hohenegger, C., Jahns, T., Kloster, S., Kinne, S., Lasslop, G., Kornblueh, L., Marotzke, J., Matei, D., Meraner, K., Mikolajewicz, U., Modali, K., Müller, W., Nabel, J., Notz, D., Peters, K., Pincus, R., Pohlmann, H., Pongratz, J., Rast, S., Schmidt, H., Schnur, R., Schulzweida, U., Six, K., Stevens, B., Voigt, A., and Roeckner, E.: DKRZ MPI-ESM1.2-HR model output prepared for CMIP6 ScenarioMIP ssp585, 10.22033/ESGF/CMIP6.4403, 2019a.

Schupfner, M., Wieners, K.-H., Wachsmann, F., Steger, C., Bittner, M., Jungclaus, J., Früh, B., Pankatz, K., Giorgetta, M., Reick, C., Legutke, S., Esch, M., Gayler, V., Haak, H., de Vrese, P., Raddatz, T., Mauritsen, T., von Storch, J.-S., Behrens, J., Brovkin, V., Claussen, M., Crueger, T., Fast, I., Fiedler, S., Hagemann, S., Hohenegger, C., Jahns, T., Kloster, S., Kinne, S., Lasslop, G., Kornblueh, L., Marotzke, J., Matei, D., Meraner, K., Mikolajewicz, U., Modali, K., Müller, W., Nabel, J., Notz, D., Peters-von Gehlen, K., Pincus, R., Pohlmann, H., Pongratz, J., Rast, S., Schmidt, H., Schnur, R., Schulzweida, U., Six, K., Stevens, B., Voigt, A., and Roeckner, E.: DKRZ MPI-ESM1.2-HR model output prepared for CMIP6 ScenarioMIP ssp126, 10.22033/ESGF/CMIP6.4397, 2019b.

Séférian, R.: CNRM-CERFACS CNRM-ESM2-1 model output prepared for CMIP6 CMIP historical, 10.22033/ESGF/CMIP6.4068, 2018a.

Séférian, R.: CNRM-CERFACS CNRM-ESM2-1 model output prepared for CMIP6 CMIP piControl, Earth System Grid Federation [dataset], 10.22033/ESGF/CMIP6.4165, 2018b.

Seibel, B. A.: Critical oxygen levels and metabolic suppression in oceanic oxygen minimum zones, Journal of Experimental Biology, 214, 326-336, 10.1242/jeb.049171, 2011.

Seibel, B. A. and Birk, M. A.: Unique thermal sensitivity imposes a cold-water energetic barrier for vertical migrators, Nature Climate Change, 12, 1052-1058, 10.1038/s41558-022-01491-6, 2022.

Seibel, B. A., Andres, A., Birk, M. A., Burns, A. L., Shaw, C. T., Timpe, A. W., and Welsh, C. J.: Oxygen supply capacity breathes new life into critical oxygen partial pressure (Pcrit), Journal of Experimental Biology, 224, jeb242210, 10.1242/jeb.242210, 2021.

Sharp, J. D., Fassbender, A. J., Carter, B. R., Johnson, G. C., Schultz, C., and Dunne, J. P.: GOBAI-O2: temporally and spatially resolved fields of ocean interior dissolved oxygen over nearly two decades, Earth Syst. Sci. Data Discuss., 2022, 1-46, 10.5194/essd-2022-308, 2022.

Stramma, L., Schmidtko, S., Bograd, S. J., Ono, T., Ross, T., Sasano, D., and Whitney, F. A.: Trends and decadal oscillations of oxygen and nutrients at 50 to 300 m depth in the equatorial and North Pacific, Biogeosciences, 17, 813-831, 10.5194/bg-17-813-2020, 2020.

Swart, N. C., Cole, J. N. S., Kharin, V. V., Lazare, M., Scinocca, J. F., Gillett, N. P., Anstey, J., Arora, V., Christian, J. R., Jiao, Y., Lee, W. G., Majaess, F., Saenko, O. A., Seiler, C., Seinen, C., Shao, A., Solheim, L., von Salzen, K., Yang, D., Winter, B., and Sigmond, M.: CCCma CanESM5 model output prepared for CMIP6 CMIP historical, 10.22033/ESGF/CMIP6.3610, 2019a.

Swart, N. C., Cole, J. N. S., Kharin, V. V., Lazare, M., Scinocca, J. F., Gillett, N. P., Anstey, J., Arora, V., Christian, J. R., Jiao, Y., Lee, W. G., Majaess, F., Saenko, O. A., Seiler, C., Seinen, C., Shao, A., Solheim, L., von Salzen, K., Yang, D., Winter, B., and Sigmond, M.: CCCma CanESM5 model output prepared for CMIP6 ScenarioMIP ssp585, 10.22033/ESGF/CMIP6.3696, 2019b.

Swart, N. C., Cole, J. N. S., Kharin, V. V., Lazare, M., Scinocca, J. F., Gillett, N. P., Anstey, J., Arora, V., Christian, J. R., Jiao, Y., Lee, W. G., Majaess, F., Saenko, O. A., Seiler, C., Seinen, C., Shao, A., Solheim, L., von Salzen, K., Yang, D., Winter, B., and Sigmond, M.: CCCma CanESM5 model output prepared for CMIP6 CMIP piControl, Earth System Grid Federation [dataset], 10.22033/ESGF/CMIP6.3673, 2019c.

Swart, N. C., Cole, J. N. S., Kharin, V. V., Lazare, M., Scinocca, J. F., Gillett, N. P., Anstey, J., Arora, V., Christian, J. R., Jiao, Y., Lee, W. G., Majaess, F., Saenko, O. A., Seiler, C., Seinen, C., Shao, A., Solheim, L., von Salzen, K., Yang, D., Winter, B., and Sigmond, M.: CCCma CanESM5 model output prepared for CMIP6 ScenarioMIP ssp126, Earth System Grid Federation [dataset], 10.22033/ESGF/CMIP6.3683, 2019d.

Tai, T. C., Calosi, P., Gurney-Smith, H. J., and Cheung, W. W. L.: Modelling ocean acidification effects with life stage-specific responses alters spatiotemporal patterns of catch and revenues of American lobster, Homarus americanus, Scientific Reports, 11, 23330, 10.1038/s41598-021-02253-8, 2021.

Tang, Y., Rumbold, S., Ellis, R., Kelley, D., Mulcahy, J., Sellar, A., Walton, J., and Jones, C.: MOHC UKESM1.0-LL model output prepared for CMIP6 CMIP piControl, Earth System Grid Federation [dataset], 10.22033/ESGF/CMIP6.6298, 2019a.

Tang, Y., Rumbold, S., Ellis, R., Kelley, D., Mulcahy, J., Sellar, A., Walton, J., and Jones, C.: MOHC UKESM1.0-LL model output prepared for CMIP6 CMIP historical, 10.22033/ESGF/CMIP6.6113, 2019b.

Taylor, C. D.: The effect of pressure upon the solubility of oxygen in water: Implications of the deviation from the ideal gas law upon measurements of fluorescence quenching, Archives of Biochemistry and Biophysics, 191, 375-384, https://doi.org/10.1016/0003-9861(78)90101-7, 1978.

Tittensor, D. P., Novaglio, C., Harrison, C. S., Heneghan, R. F., Barrier, N., Bianchi, D., Bopp, L., Bryndum-Buchholz, A., Britten, G. L., Büchner, M., Cheung, W. W. L., Christensen, V., Coll, M., Dunne, J. P., Eddy, T. D., Everett, J. D., Fernandes-Salvador, J. A., Fulton, E. A., Galbraith, E. D., Gascuel, D., Guiet, J., John, J. G., Link, J. S., Lotze, H. K., Maury, O., Ortega-Cisneros, K., Palacios-Abrantes, J., Petrik, C. M., du Pontavice, H., Rault, J., Richardson, A. J., Shannon, L., Shin, Y.-J., Steenbeek, J., Stock, C. A., and Blanchard, J. L.: Next-generation ensemble projections reveal higher climate risks for marine ecosystems, Nature Climate Change, 11, 973-981, 10.1038/s41558-021-01173-9, 2021.

Tokarska, K. B., Stolpe, M. B., Sippel, S., Fischer, E. M., Smith, C. J., Lehner, F., and Knutti, R.: Past warming trend constrains future warming in CMIP6 models, Science Advances, 6, eaaz9549, doi:10.1126/sciadv.aaz9549, 2020.

Vaquer-Sunyer, R. and Duarte, C. M.: Thresholds of hypoxia for marine biodiversity, Proceedings of the National Academy of Sciences, 105, 15452-15457, 10.1073/pnas.0803833105, 2008.

Verberk, W. C. E. P., Bilton, D. T., Calosi, P., and Spicer, J. I.: Oxygen supply in aquatic ectotherms: Partial pressure and solubility together explain biodiversity and size patterns, Ecology, 92, 1565-1572, https://doi.org/10.1890/10-2369.1, 2011.

Voldoire, A.: CNRM-CERFACS CNRM-ESM2-1 model output prepared for CMIP6 ScenarioMIP ssp126, Earth System Grid Federation [dataset], 10.22033/ESGF/CMIP6.4186, 2019a.

Voldoire, A.: CNRM-CERFACS CNRM-ESM2-1 model output prepared for CMIP6 ScenarioMIP ssp585, Earth System Grid Federation [dataset], 10.22033/ESGF/CMIP6.4226, 2019b.

von Schuckmann, K., Cheng, L., Palmer, M. D., Hansen, J., Tassone, C., Aich, V., Adusumilli, S., Beltrami, H., Boyer, T., Cuesta-Valero, F. J., Desbruyères, D., Domingues, C., García-García, A., Gentine, P., Gilson, J., Gorfer, M., Haimberger, L., Ishii, M., Johnson, G. C., Killick, R., King, B. A., Kirchengast, G., Kolodziejczyk, N., Lyman, J., Marzeion, B., Mayer, M., Monier, M., Monselesan, D. P., Purkey, S., Roemmich, D., Schweiger, A., Seneviratne, S. I., Shepherd, A., Slater, D. A., Steiner, A. K., Straneo, F., Timmermans, M. L., and Wijffels, S. E.: Heat stored in the Earth system: where does the energy go?, Earth Syst. Sci. Data, 12, 2013-2041, 10.5194/essd-12-2013-2020, 2020.

Weiss, R. F. and Price, B. A.: Nitrous oxide solubility in water and seawater, Marine Chemistry, 8, 347-359, https://doi.org/10.1016/0304-4203(80)90024-9, 1980.

Whalen, M. A., Whippo, R. D. B., Stachowicz, J. J., York, P. H., Aiello, E., Alcoverro, T., Altieri, A. H., Benedetti-Cecchi, L., Bertolini, C., Bresch, M., Bulleri, F., Carnell, P. E., Cimon, S., Connolly, R. M., Cusson, M., Diskin, M. S., D'Souza, E., Flores, A. A. V., Fodrie, F. J., Galloway, A. W. E., Gaskins, L. C., Graham, O. J., Hanley, T. C., Henderson, C. J., Hereu, C. M., Hessing-Lewis, M., Hovel, K. A., Hughes, B. B., Hughes, A. R., Hultgren, K. M., Jänes, H., Janiak, D. S., Johnston, L. N., Jorgensen, P., Kelaher, B. P., Kruschel, C., Lanham, B. S., Lee, K.-S., Lefcheck, J. S., Lozano-Álvarez, E., Macreadie, P. I., Monteith, Z. L., O'Connor, N. E., Olds, A. D., O'Leary, J. K., Patrick, C. J., Pino, O., Poore, A. G. B., Rasheed, M. A., Raymond, W. W., Reiss, K., Rhoades, O. K., Robinson, M. T., Ross, P. G., Rossi, F., Schlacher, T. A., Seemann, J., Silliman, B. R., Smee, D. L., Thiel, M., Unsworth, R. K. F., van Tussenbroek, B. I., Vergés, A., Yeager, M. E., Yednock, B. K., Ziegler, S. L., and Duffy, J. E.: Climate drives the geography of marine consumption by changing predator communities, Proceedings of the National Academy of Sciences, 117, 28160-28166, doi:10.1073/pnas.2005255117, 2020.

Zweng, M. M., Reagan, J. R., Seidov, D., Boyer, T. P., Locarnini, R. A., Garcia, H. E., Mishonov, A. V., Baranova, O. K., Weathers, K. W., Paver, C. R., and Smolyar, I. V.: World Ocean Atlas 2018, Volume 2: Salinity. A. Mishonov Technical Ed., NOAA Atlas NESDIS 82, 50 pp., 2019.